Fall 2016

Lysosomal reacidification by degradation of poly(dl-lactide-CO-glycolide) nanoparticles in a lipotoxic cardiomyopathy model

Frederick Martin Zasadny
University of Iowa

LYSOSOMAL REACIDIFICATION BY DEGRADATION OF POLY(DL-LACTIDE-CO-GLYCOLIDE) NANOPARTICLES IN A LIPOTOXIC CARDIOMYOPATHY MODEL

by

Frederick Martin Zasadny

A thesis submitted in partial fulfillment
of the requirements for the Master of Science
degree in Biomedical Engineering in the
Graduate College of
The University of Iowa

December 2016

Thesis Supervisor: Professor E. Dale Abel

Graduate College
The University of Iowa
Iowa City, Iowa

CERTIFICATE OF APPROVAL

_____

MASTER'S THESIS

_____

This is to certify that the Master's thesis of

Frederick Martin Zasadny

has been approved by the Examining Committee for
the thesis requirement for the Master of Science degree
in Biomedical Engineering at the December 2016 graduation.

Thesis Committee: _____
E. Dale Abel, Thesis Supervisor

_____
James A. Ankrum

_____
Michael A. Mackey

To those who have guided my thinking to present a clear interpretation of data.

ACKNOWLEDGEMENTS

I would like to thank my direct and indirect mentors throughout my time in the Abel Laboratory at the University of Iowa, specifically Drs. Renata Pereira, Bharat Jaishy, Kensuke Tsushima, James Ankrum and E. Dale Abel. I especially would like to thank Dr. Abel for the opportunity to conduct research in his laboratory. I am very fortunate to have experienced and learned from his extremely rigorous scientific method.

I also would like to acknowledge my committee members, Drs. James Ankrum, Michael Mackey and E. Dale Abel for providing constructive criticism in the writing of this thesis.

ABSTRACT

Lipotoxic cardiomyopathy increases the risk of heart failure in obese patients by adversely altering heart structure and function *via* toxic lipid specie mediated cellular stress and cell death [1]. Increased fatty acid uptake and esterification in cardiomyocytes increases toxic lipid intermediates [2]. These cardiotoxic lipid species such as diacylglycerol have recently been shown to deacidify lysosomes in cardiomyocytes by activating protein kinase C βII mediated NADPH oxidase 2 generation of superoxide that inhibits proton pumps on lysosomal membranes by S-nitrosylation [3]. Autophagy, a lysosome dependent cellular survival process, is impaired upon cardiomyocyte lipid-overload due to inhibition of pH-dependent proteolytic autophagosome degradation in the lysosome. Subsequent accumulation of autophagic vesicles heightens cardiomyocyte sensitization to additional stresses of ischemia-reperfusion or ER dysfunction, culminating in impaired cardiac metabolic flexibility leading to cell death. Low cardiomyocyte regenerative capacity calls for strategies to preserve cell number in states of increased stress, such as lipid-induced impairment of autophagy [4]. Lysosome-targeted reacidifying devices can provide an effective means to restore autophagic flux [5-7].

In this thesis, a therapeutic strategy utilizing poly(DL-lactide-co-glycolide) (PLGA) nanoparticle degradation to reacidify lysosomes and revert cardiotoxic lipid specie induced blockade in autophagic flux in cardiomyocytes is presented. Endocytosed PLGA acidic nanoparticles were designed to rapidly degrade and release acidic monomers in lysosomes to restore pH dependent phosphatase and cathepsin L activity in cardiomyocytes with acute lipotoxicity. Optimized pre-palmitate treatment periods demonstrated that PLGA nanoparticles with polyethylenimine cationic surface coatings provide an effective restoration of autophagic flux in the presence of lipid-overload modeled by acute palmitate treatment in cardiomyocytes.

PUBLIC ABSTRACT

With the onset of accessible fatty diets in cultures globally, cardiovascular related deaths have risen to the leading mortality worldwide. Excess fat supply increases fat buildup in heart muscle and produces toxic molecules that cause fundamental changes to heart structure and function. Specifically, generation of reactive oxygen inhibit a 'self-eating' cellular survival process known as autophagy by deacidifying lysosomes in heart muscle cells. Blocked autophagy is detrimental to heart structure and function by increasing cell death. Autophagic inflexibility due to increased fat-derived toxic molecules contributes to cardiac fragility and subsequently increases heart failure in instances of additional stress to the heart, such as a heart attack. Devices designed to release acid upon delivery to the lysosome could restart autophagy and reduce the potential for heart failure. The FDA approved acidic biomaterial poly(DL-lactide-co-glycolide) is an attractive building block from which these devices can be made. A proof-of-principle reacidification of lysosomes for restored autophagy and long-term prevention of heart failure in obese patients is demonstrated in this thesis.

TABLE OF CONTENTS

LIST OF TABLES

LIST OF FIGURES

Section I Introduction

I.1 Need Based Lipotoxic Cardiomyopathy Intervention

Lipotoxicity (lipid-overload) is a cellular state of impaired function due to the accumulation of ectopic lipid in tissues not designed to store large amounts of fatty acid in the form of triacylglycerol and various toxic lipid intermediates such as ceramide and diacylglycerol that perturb cellular survival [10]. The accumulation of lipid in these tissues, such as heart and liver, is caused by consistent presentation of lipid to the cell from increased circulating fatty acid levels, as seen in obesity and the metabolic syndrome.

Cardiomyocyte (CM) lipid-overload is observed in patients presenting obesity (body mass index >30) and/or type 2 diabetes (T2D) as well as the metabolic syndrome. In these patients, left ventricular dysfunction and decompensated hypertrophy contribute to decreased ejection fraction that quickly leads to heart failure. Lipid-overload in CMs is believed to contribute to observed CM death and decreased heart function by perturbing insulin signaling, mitochondrial function and autophagic flux, and is thus termed lipotoxic cardiomyopathy [10-12].

Blocked autophagic flux observed upon lipid-overload in CMs increases the sensitization of CMs to cellular stress, leading to apoptosis. In areas of increased CM apoptosis, increased fibrosis stiffens the heart's structure leading to decompensated hypertrophy that leads to heart failure. Additionally, low CM regenerative capacity calls for strategies to preserve cell number in the adult heart in states of increased cellular stress [4].

Due to the rising prevalence of obesity in cultures worldwide where 600 million adults present obesity, there is a **need** to directly modulate the adverse effects of lipid-overload in the heart, preventing lipotoxic cardiomyopathy and heart failure [13, 14]. Treatments of cardiac lipotoxicity can have far-reaching effects by improving patient quality of life as well as

reducing heart failure. Constitutive benefits of reduced economic burden and increased life expectancy can bring about a new age of medicine, where heart failure is not the leading cause of death. A proof-of-principle CM therapy to revert lipid-overload impairment of lysosomal acidification and subsequent autophagic flux is laid out in this thesis for a Master of Science degree in biomedical engineering.

Section II Physiology

II.1 Lipotoxic Cardiomyopathy

Obesity is rigorously known to be an independent risk factor in cardiovascular diseases [15-17]. In patients presenting obesity and the metabolic syndrome, the heart is exposed to high extracellular lipid concentrations in the form of circulating albumin bound fatty acid and triglyceride contained in very low density lipoprotein (VLDL) particles and chylomicrons. This is a consequence of exhausted lipid droplet storage in white adipose tissue. Imbalance in nutrient intake and expenditure overload adipose storage capacity, causing a lipid storage shunt to tissues not designed for increased cellular lipid deposition, such as skeletal muscle, liver, kidney, vascular endothelium, pancreas and heart [10].

Lipotoxicity in the heart is driven by the abnormal accumulation of lipid in CMs, particularly the accumulation of reactive lipid moieties derived from the partial completion of perturbed oxidative and non-oxidative lipid pathways of anabolism and catabolism. When bathed in high concentrations of fatty acid, CMs increase fatty acid uptake through fatty acid stimulation of fatty acid translocases, such as CD36 [18]. Once in the cell, fatty acids are esterified to coenzyme A (CoA). The resulting fatty acyl-CoA is processed for energy production in the mitochondria (β-oxidation), membrane biosynthesis (phospholipids) or conversion to

triacylglycerol (TG) for storage. Lipotoxicity occurs when these processes are inhibited or saturated with too much fatty acid, such as exhausted mitochondrial β-oxidation capacity. In addition to saturated β-oxidation rates, lipid-overload inhibited TG synthesis from fatty acyl-CoA leads to an accumulation of toxic lipid intermediates such as diacylglycerol (DAG), ceramide, long-chain acyl-CoA, and acylcarnitines [11]. These intermediates, especially DAG, are considered toxic due to their disruption of signal transduction pathways, particularly insulin signaling, leading to insulin resistance and ultimately CM death and heart failure [19]. As such, lipotoxic cardiomyopathy is as disease where the increased ectopic deposition of lipid in the heart increases the risk of production of reactive lipid moieties that cause cell death via altered cellular signaling, mitochondrial dysfunction, ER-stress, impaired autophagic flux and oxidative damage [10, 20].

Fatty acids primarily serve as carbon substrates for CM ATP production. CMs oxidize fatty acids derived from the unpacking of TG in a process called β-oxidation. Due to constant hemodynamic loads to drive blood through the systemic vasculature, the rate of β-oxidation and glucose oxidation in CMs are significantly higher than less metabolically active tissues such as fat. Specifically, the heart turns over its ATP content {5umol/g wet wt} every 10 seconds [21, 22]. As such, there is a high demand for carbon substrate (glucose, lactate, ketones, amino acid, and fatty acid). Interestingly, the heart prefers fatty acid to other substrates as its main carbon source in ATP production in a highly balanced mitochondrial β-oxidation regulation program dependent on cardiac workload, substrate availability, oxygen supply and neurohormonal modulation [23, 24]. In β-oxidation, sequentially catalyzed removal of two carbon units from fatty acyl-CoA to form acetyl-CoA drives tricarboxylic acid cycle reduction of nicotinamide adenine dinucleotide (NAD) and flavin adenine dinucleotide (FAD) for the reduction of electron

transport chain complexes, building a mitochondrial electrochemical gradient for ATP production.

Stimulated translocation of fatty acid transporters CD36 and FATB1 by high extracellular lipid levels increase the intracellular pool of lipids. As mentioned previously, the lipotoxic state is evident in CMs when there is an imbalance in the rates of uptake, oxidation, and storage of fatty acids. Importantly, lipid packaging (esterification) events in the cytosol also dictate the potent side effects of lipid-overload. For example, impaired triglyceride synthesis produces bioactive lipid intermediates such as DAG that disrupt fatty acid oxidation transcriptional programs (such as PPARα [25]) and post-translational modification of proteins, leading to ER stress, mitochondrial dysfunction, apoptosis, and inhibited autophagy. Thus, lipotoxicity is a multifaceted organ-specific result of cytosolic lipid misuse caused by increased presentation of lipid.

Importantly, increased fatty acid oxidation and reduced glucose oxidation in the heart precedes mitochondrial dysfunction seen in cardiac lipotoxicity, indicating that oxidative substrate switch may be the initiator of adaptive signaling pathways (such as in states of compensated hypertrophy) which progress to maladaptive processes (such as in states of heart failure) [12]. Cardiac steatosis is the result of the storage of ectopic lipid in the form of relatively inert triglyceride or potent bioactive lipid intermediates ceramide and DAG. These bioactive lipid-based macromolecules then dictate the progression of chronic cardiac lipotoxicity, which presents **reduced** fatty acid oxidation, **increased** mitochondrial dysfunction, ER stress, apoptosis and **impaired** autophagic flux.

II.2 Autophagy in the Heart

Macroautophagy (hereafter autophagy) is an intracellular catabolic process initiated in CMs by metabolic and survival stresses, such as the fasting state [26]. Multiple signaling pathways converge on autophagy for cellular housekeeping (removing toxic protein aggregates or damaged organelles) and cellular metabolic homeostasis (producing carbon-based metabolites by degrading organelles, proteins, membranes, carbohydrates, and lipids). This process of self-catabolism for anabolism or energy production enable the cell to quickly adapt to spatio-temporal stresses [27].

Inhibition of the mammalian target of rapamycin (mTOR) initiates autophagy. Specifically, inhibition of the mTOR complex 1 (mTORC1) in states of cellular nutrient deprivation, such as reduced amino acid and glucose levels, has been well documented to activate autophagy for subsequent metabolite production, as well as reduced mTORC1-initiated protein production [28-30]. mTORC1 acts as a major nutrient sensor, responding to growth factors and metabolic signaling such as the AMP activated protein kinase (AMPK)-initiated signal transduction for cellular growth and survival. These metabolic sensing and signaling pathways activate autophagy when energy levels are low.

Autophagy is a master energy redistribution process by engulfing organelles, membranes, lipids, carbohydrates, and protein aggregates through the formation of a phagophore that matures into a double membrane carrier vesicle called an autophagosome. This autophagosome is trafficked to the lysosome, where upon fusion and formation of the autolysosome lysosomal hydrolases degrade autophagic cargo as well as the double membrane carrier vesicle, producing metabolites and protein synthesis building blocks. The passage of the autophagosome through CMs from formation to degradation is termed autophagic flux. The degradation of lipids (lipophagy [31]),

carbohydrates (glycophagy [32-35]), mitochondria (mitophagy [36]) and even iron (ferritinophagy [37]), produce a milieu of metabolites and building blocks to promote cellular adaptation to stress and nutrient deprivation states [27]. Chronic inhibition of autophagy leads to type II cell death (autophagy mediated), as opposed to necrotic or apoptotic cell death [38]. This cell death is characterized by the extensive accumulation of autophagosomes [39].

As discussed above, **intracellular levels of bioactive lipids modulate autophagy** [3, 10]. Importantly, the role of lipid-overload in modulating autophagy is bi-phasic. Namely, concentrations of palmitate (C16:0 saturated fatty acid) slightly above physiologic levels **induce autophagy** in CMs subsequent to ER stress in a possible adaptive and cardioprotective mechanism [40]. Cardioprotective mechanisms induced by palmitate may also involve increased lipophagy, which increases the clearance of lipids by mobilizing the lipid stores in various cell types, albeit not shown in cardiomyocytes directly due to the small amount of lipid stores present at normo-physiological levels [10]. **However**, upon presentation of higher levels of palmitate (500uM), **autophagy is impaired**; most likely due to the acute activation of superoxide generation through DAG mediated protein kinase C βII overactivation of NADPH oxidase 2 (NOX2). This extra-mitochondrial superoxide generation was shown to S-nitrosylate lysosomal ATP-dependent V-type H^+ ATPase (vATPase), which subsequently deacidified lysosomes and impaired lysosomal pH dependent hydrolase degradation of autophagosomes indicating the mechanistic link between lipotoxicity and blocked autophagic flux [3]. Therefore, the initiation of autophagy upon presentation of sub-toxic concentrations of palmitate is blunted by maladaptive superoxide generation caused by toxic concentrations of bioactive lipid intermediates produced by impaired or saturated TG synthesis and saturated rates of β-oxidation

when high levels of lipid are available to CMs. Increased availability of these bioactive lipid species impair lysosomal autophagosome degradation [3].

In this thesis, the acute presentation (4 hours) of toxic levels (500uM) of palmitate (C16:0) modeled an acute lipotoxic state, proven by the restoration in autophagic flux upon removal of extracellular palmitate in cultured CMs after a 4 hour treatment [3]. Acute lipotoxicity is considered an understanding of the early effects of toxic concentrations of lipid on the CM and may be a summation of adaptive-to-maladaptive processes that sensitize the CM to cell death, leading to ventricular dysfunction and heart failure. The acute effect of toxic concentrations of saturated fatty acid perturbs autophagy in a superoxide dependent manner by inhibiting lysosomal proton pumps, leading to impaired autophagosome turnover [3]. This thesis considers the modulation of the observed inhibition of autophagic flux in the acute lipotoxic state in CMs by using a proof-of-principle approach of reacidification of lysosomes by the degradation of poly(DL-lactide-co-glycolide) acidic nanoparticles.

Section III Modulating pH

III.1 Lysosomal pH

The lysosome is an intracellular organelle with degradative and signaling functions. The lysosome is constructed of a single lipid membrane bound lumen containing hydrolases necessary for the degradation and recycling of cargo delivered by the endosomal and autophagic pathways.

Lysosomes contain ~60 catabolic enzymes that function optimally at an acidic pH [41]. Many of these endoplasmic reticulum derived, pH dependent enzymes are trafficked to the lysosome from the Golgi complex and are post translationally modified by the mannose-6-phosphate (M6P) pathway [41]. Additionally, the presence of mannose-6-phosphate receptors, a type 1

transmembrane glycoprotein, allows the differentiation of lysosomal compartments from that of the endosomal pathway compartments [41]. These receptors bind the M6P bound hydrolase complex, and thereby allow selective concentration and activation of hydrolases in the acidic lumen of the lysosome. To keep the membrane of the lysosome intact in the presence of these catabolic enzymes, the polysaccharide glycocalyx thickly coats the luminal side of the lysosomal membrane to resist digestion [42].

Lysosomal enzyme activity remains optimal at a pH range of 4.5-5 due to adequate active site protonation [43-45]. Luminal reduction in pH is achieved through vATPase proton pumps on the membranes of late endosomes and lysosomes. Two subunits of the vATPase complex enable the coupling of hydrolytic cleavage of ATP to ADP to subsequently transport two protons into the lysosomal lumen. Upon energy release of ATP at the cytosolic V1 subunit, the rotor structure of V1 turns in the membrane bound V0 subunit, allowing for direct proton movement from the cytosol to the lumen of the lysosome [46]. These two subunits are reversibly assembled, allowing for **regulation of lysosomal pH** [47, 48].

Membrane bound proteins on the lysosome enable the fusion of autophagosomes and late endosomes to the lysosome, linking the subcellular trafficking processes of autophagy and endocytosis to their final destination and function. Lysosomal membrane proteins enable fusion of autophagosomes to lysosomes for **pH dependent autophagosome degradation**.

The degradative potential of the lysosome enables the recycling of proteins and organelles to feed anabolic processes of cell survival, such as the degradation of autophagosomes to produce amino acids for protein synthesis or lipids for membrane formation. In this way, the lysosome is an integral player in the cell survival response of both metabolic stresses and toxic cargo clearance.

Dysfunctional lysosomes inhibit the degradation of cargo and lead to lysosomal storages diseases, such as Danon disease where absence of lysosome-associated membrane protein 2 (LAMP2) in an X-linked dominant mutation causes autophagosome accumulation seen in cardiac and skeletal muscle tissue [49]. In this disease, the deficiency in LAMP2, specifically isoform LAMP2B, on the membrane leads to excessive vacuolization of cardiac tissue (Figure 1), an effect thought to be the result of defective autophagosome binding to and degradation in lysosomes [8].

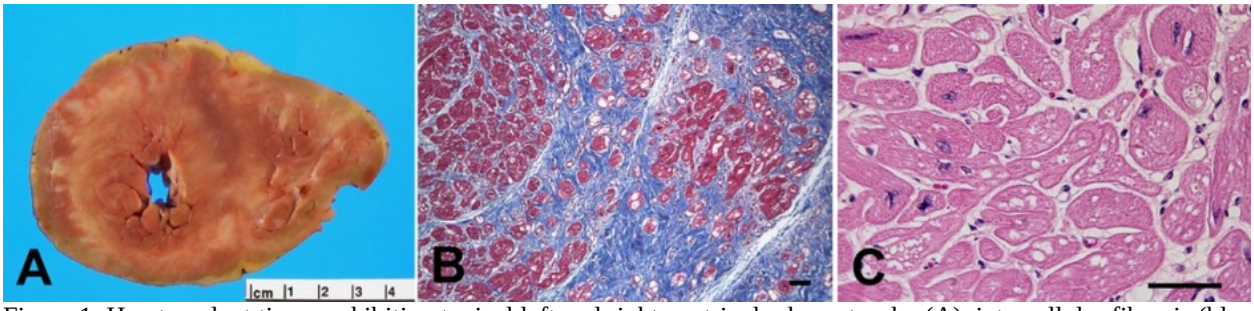

Figure 1: Heart explant tissue exhibiting typical left and right ventricular hypertrophy (A), intercellular fibrosis (blue areas in trichrome stain) (B) and excessive vacuolization (clear areas in hematoxylin and eosin staining) (C) from a 14-old-male with Danon disease [8].

Not only can lysosomal fusion to intracellular trafficking vesicles be inhibited, as seen in Danon disease, but also the degradative function of lysosomes can be directly perturbed causing a milieu of toxic lysosomal storage disease phenotypes. The autophagy-lysosome degradative pathway is inhibited in Parkinson's disease by dysregulation of lysosomal pH, representing a plausible major neurotoxic player in the generation of neurodegenerative diseases [50]. In Parkinson's disease, the mutation driven deficiency of ATP13A2 gene leads to lysosomal deacidification as well as membrane instability [50]. Reduced cargo/substrate processing of lysosomal hydrolases upon increased pH is thought to contribute to the observed blocked autophagosome clearance and subsequently sensitize neurons to apoptosis [50]. Importantly, Bourdenx *et al.* reversed lysosomal degradative impairment from increased luminal pH by delivering acidic poly(DL-lactide-co-glycolide) (PLGA) nanoparticles to lysosomes to decrease the pH and restore

degradative hydrolase activity in ATP13A2 L3292 fibroblasts [7]. Interestingly, PLGA nanoparticle intracerebral injections in mice protected neurons from MPTP-induced cell death (MPTP is a molecule responsible for modeling disrupted lysosomal integrity and function seen in Parkinson's disease) by restoring lysosomal acid phosphatase 2 activity (Figure 2) [7].

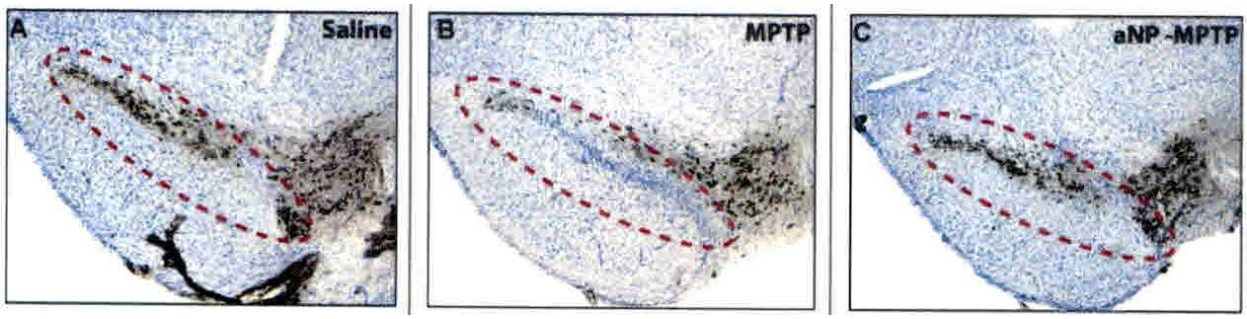

Figure 2: Mouse dopaminergic neurons TH-immunostained (dark regions in dotted region) (A) protected against MPTP induced lysosome dysfunction related cell death (B) by injections of PLGA nanoparticles (C) [7].

III.2 Poly(DL-lactide-co-glycolide) (PLGA) Acidic Nanoparticles

Reacidifying lysosomes to restore degradative capacity and subsequent intracellular recycling processes such as autophagy in CM's is the key component in this thesis. This need springs from the newly identified mechanism of lipid-overload induced NOX2 mediated lysosomal deacidification in CM's, leading to increased sensitization to ER stress and CM death through the accumulation of autophagic vesicles and subsequent reduction in metabolite production from autophagy.

Recently, several studies have identified endocytosed PLGA nanoparticles as a therapeutic **lysosomal reacidifier upon degradation** in various cell types and disease states [5-7]. These studies have probed uptake and reacidification profiles of PLGA nanoparticles by utilizing available methods of fluorescent pH measurement and lysosomal enzyme activity. In one such study, PLGA was shown to traffic to lysosomes of immortalized human retinal pigment epithelial (RPE) cells within 1 hour. Additionally, reacidification of lysosomal luminal space

was detected at 1 hour up to 12 days even in the presence of chloroquine, a lysosomotropic weak base that increases lysosomal pH. Enzyme activity detected by substrate binding to cathepsin D was also enhanced in PLGA nanoparticle treated cells [6]. This study formed the foundation from which the following hypothesis was tested.

Hypothesis: It is possible to restore CM lysosomal pH for optimal enzyme activity, which will restore autophagic flux, by delivering PLGA nanoparticles to lysosomes via endocytosis for degradation into acidic monomers at an adequate rate in the presence of lipid-overload induced lysosomal dysfunction.

More specifically, the following hypotheses were tested in this thesis:

1. **PLGA nanoparticles will be delivered to CM lysosomes by endocytosis.**
2. **PLGA nanoparticles in lysosomes will degrade into acidic monomers at an adequate rate to reacidify lysosomal luminal space in the presence of lipid-overload induced impairment of lysosomal acidification.**
3. **Restored CM lysosomal pH will restore lysosomal enzyme activity.**
4. **Restored CM lysosomal enzyme activity will reduce blocked autophagosome degradation.**

Since the study in RPE cells, some groups have continued to probe the use of PLGA as a lysosomal reacidifier. As mentioned earlier, Bourdenx *et al.* used PLGA nanoparticles to restore dopaminergic neuronal lysosomal pH and attenuate Parkinson disease related lysosomal storage disorder [7]. Notably, the authors also tested their PLGA nanoparticles on X-linked myopathy with excessive autophagy (XMEA)-mutant fibroblasts. Results indicate that in the presence of chloroquine, PLGA nanoparticles were able to restore lysosomal pH, but not in the presence of the vATPase inhibitor bafilomycin. The authors suggest that PLGA nanoparticles can only apply their full acidification potential when vATPase activity is partially functional [7].

In another study by Trudeau *et al.*, increases in INS1 insulinoma cell lysosomal pH upon lipid-overload was reverted upon light stimulated acid release from customized nanoparticles [5].

Restored lysosomal pH was reported to restore autophagic flux, albeit without the proper mCherry-GFP-LC3 fluorescent imaging experiments or chloroquine controls. The reported effect suggested a more robust effect than that of PLGA nanoparticles tested in parallel. This study invigorated this current thesis work by providing direct evidence that lysosomal pH can be modulated with controlled acid release to restore autophagic flux in the presence of lipid-overload.

Section IV Models

IV.1 Acute Lipotoxic Cardiomyopathy

As described earlier, the **acute effect** of toxic concentrations of saturated fatty acid can perturb autophagy in a superoxide dependent manner, where lysosomal proton pumps are inhibited leading to impaired autophagosome turnover [3]. This model was replicated in this thesis due to the non-cytotoxic nature of lipid-overload at the reported timeline, which allows a better view of autophagic flux rescue, i.e. without the context of cell death. Specifically, the addition of high levels of palmitate (C16:0), a highly common saturated fatty acid and implicated to cause lipid-overload, applied to differentiated immortalized H9c2 rat cardiomyoblasts (CMs) in the presence of low concentrations of glucose (5.55mM) for 4 hours produces a reversible blockade in autophagic flux. The reversibility in blocked autophagosome degradation upon removal of palmitate indicates that this model is non-cytotoxic and is therefore an adequate model to study the effects of lipid-overload, without the additional effects of palmitate induced cell death seen at later time points [3]. This acute lipid-overload model of impaired autophagy allows probing of cell therapies to modulate autophagy in the presence of high levels of palmitate.

IV.2 PLGA Nanoparticle Design

As discussed above, several studies have shown that acidic nanoparticles constructed **solely** of poly(DL-lactide-co-glycolide) (PLGA) can reacidify lysosomes in various disease models, further demonstrating the advantages of PLGA as a platform **itself** for cellular therapies [5-7]. Indeed, PLGA has been extensively tested in drug delivery systems due to highly modifiable properties for controlled release of hydrophilic and hydrophobic drugs [9]. Additionally, PLGA is a very attractive drug delivery platform due to the biocompatibility of its byproducts, producing CO2 and H2O with intermediate protons through its hydrolysis into metabolic intermediates of lactide and glycolide and subsequent entry into various metabolic pathways. This biocompatibility has allowed PLGA to become a FDA approved polymer for use as a drug delivery system [9].

Based on the need to reacidify lysosomes, a set of design criteria were developed for a device to target lysosomal pH modulation without enhancing the disease phenotype. These design criteria for a device to reacidify lysosomes in the presence of lipid overload are listed in Table 1. PLGA nanoparticles met the criteria of degradation to acidic monomers, controllable degradation, uptake enhancement through surface modification, size variability, biocompatibility, and cellular visualization by lipophilic fluorescent probe internalization.

Table 1: Design criteria for a device to reacidify lysosomes.

General Criteria	Specific Criteria
release acid	rapid and sustained release
localize in lysosomes	trafficked via endocytosis
biocompatible	byproducts metabolized
amenable to lysosome biology	non-disruptive, small sized
uptake visualized	encapsulation of fluorescent probe

PLGA erodes by bulk degradation, whereby hydrolysis of surface **and** internal PLGA bonds produce a porous and dissolving polymeric nanoparticle. PLGA degrades into glycolic acid (pKa 3.83) and DL-lactic acid (pKa 3.86) via acid-catalyzed hydrolysis, where a water molecule aided by excess protons cleaves an ester bond between the DL-lactic acid and glycolic acid monomers (Figure 3).

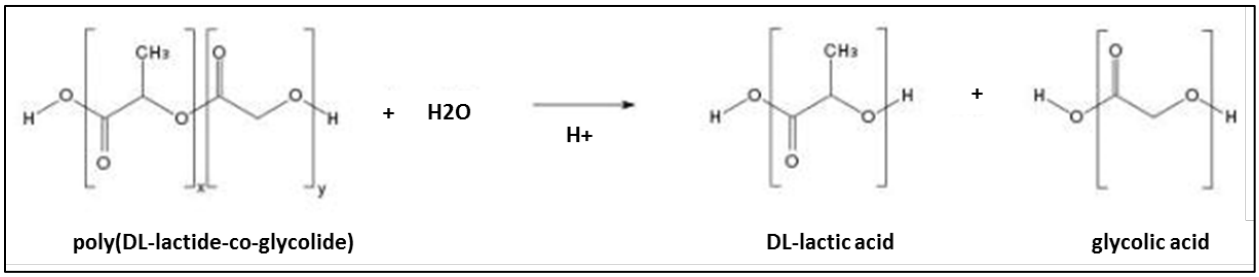

Figure 3: Poly(DL-lactide-co-glycolide) random block copolymer degrading by acid catalyzed hydrolysis into DL-lactic and glycolic acidic monomers. Modified from [9].

The DL-lactic acid and glycolic acid monomers stabilize the tetrahedral intermediates of hydrolysis by protonation, furthering hydrolysis by autocatalysis [51]. The pH microenvironment within PLGA excessively modulates the degradation rate of PLGA, through this mechanism of autocatalysis. Specifically, as more and more acidic oligomers are created from cleaved chains of PLGA within the PLGA nanoparticle, local regions of low pH accelerate the acid-catalyzed hydrolysis of additional, tightly packed lengths of polymer. This cycle repeats until the nanoparticle is highly porous and monomers and oligomers of acid wash out of the nanoparticle. As such, the release of acid from PLGA is dependent on the rate at which the polymer degrades, which is dependent on molecular weight, DL-lactide to glycolide polymer ratio, and the exogenous acid/aqueous environment.

This degradation rate dependent release of acid can be modified by the addition of **free glycolic acid**, whereby the addition of non-polymerized glycolic acid to the formulation of the nanoparticles can create additional entry points for water molecules by the formation of pores

due to the disruption of PLGA packing upon formulation. Free glycolic acid addition can also create a burst release of acid as well as increase autocatalysis by lowering the pH of internal microenvironments.

The molecular weight of PLGA influences its degradation rate. Polymer molecular weights are a measure of polymer length. As molecular weight decreases, the length of the average chain of polymer is decreased. As the chain of polymer decreases, it takes less hydrolysis to free the monomers and thereby increases the rate of degradation per chain. The additive effect of smaller chain hydrolysis produces a rapidly degrading nanoparticle. This is well documented in drug release from PLGA since the release of encapsulated drug cargo depends on the degradation rate of PLGA nanoparticle [52]. Specifically, drug release from PLGA, i.e. diffusion, is dependent on the molecular weight of PLGA by the application of Fick's second law, whereby decreasing molecular weight upon particle degradation increases the diffusion of the drug [52]. Here, a monotonic assumption of drug release and acid release can be made, since drug release from PLGA is dependent on degradation of the polymer, and degradation of the polymer releases acid monomers. This one-to-one relationship can guide the construction of PLGA for controlled release of acidic monomers. For this thesis, **the lower bound of PLGA molecular weight (4.6kDa) as available by the supplier was selected for most rapid release of acidic monomers and subsequent protons from PLGA**.

Selection of high **acid number** PLGA theoretically allows for the most acidic PLGA polymer, since the acid number is a measure of how much base, such as KOH, is needed to neutralize the protons released from PLGA. This measurement correlates with reduced PLGA molecular weight, and are often linked together. In this thesis, the highest available acid number PLGA

(23.7mg KOH/g PLGA) was selected for theoretically optimal/rapid proton release to rapidly reacidify lysosomes in the presence of lipid-overload.

In this thesis, **PLGA was constructed with a 50:50 ratio of DL-lactic to glycolic acid**, reported to have the most rapid degradation rate over other ratios due to optimal reduction in the crystallinity of DL lactide, a major determinant of degradation rate [9]. This PLGA is a random block copolymer, were a statistical distribution of DL lactide and glycolide oligomer and monomer units produce a resulting 50:50 mean constituent polymer proportion. Monomer crystallinity, specifically DL lactide, increases hydrophobic pockets within the nanoparticle due to an electrostatically favorable aggregation of hydrophobic DL lactide methyl side groups. This reduces water molecule access into PLGA, which decreases nanoparticle degradation. A 50:50 ratio of DL-lactic to glycolic acid produces an optimally amorphous polymer, where hydrophobic pockets are reduced to allow optimal access of water molecules for hydrolysis. Notably, if the proportion of DL lactide is decreased, glycolide crystallinity increases and subsequently reduces degradation rate.

Spherical nanoparticles were selected for PLGA delivery to the lysosomes due to spherical-shape dependent uptake through the clathrin-mediated endocytic pathway, a major endosome-to-lysosome pathway [53]. Additionally, **PLGA nanoparticles were designed with an average diameter of 200nm** to readily target the clathrin coated pits and minimize energy dependent uptake through clathrin-mediated endocytosis [53, 54].

In this thesis, **additional efforts to increase PLGA nanoparticle degradation rate consisted of diameter reduction to enable an increased surface area to volume ratio and the addition of free glycolic acid to nanoparticle formulation** as discussed earlier, with free glycolic acid theoretically captured by PLGA upon nanoparticle hardening. Increased surface area to volume

ratios seen when reducing nanoparticle diameter increases the area over which water molecules can enter the particle for bulk degradation per unit of nanoparticle volume. Thus, size reduction increases degradation rate by producing an excess of water molecules as well as allow clathrin-mediated endocytosis.

PLGA nanoparticle systems depend on cellular uptake, where the efficacy of the particle system is limited to cellular uptake past the anionic cell membrane. To increase cellular uptake dictated by electrostatic interactions of the negative cellular membrane potential, amine-terminated branched polyethylenimine (PEI) was electrostatically adsorbed to negatively charged carboxylic acid end groups on the PLGA nanoparticle surface. Carboxylic acid end groups were chosen to terminate the PLGA polymers to increase acid release and autocatalysis as well as allow for surface adsorption of cationic polymers. The resulting **positive** zeta-potential (a measure of surface charge) after cationic PEI adsorption on the nanoparticle surface enhances cellular spatiotemporal cellular nanoparticle uptake as previously reported [55].

PEI has been known to **absorb protons** *via* its amine groups (protonation of its primary, secondary and tertiary amines) [56]. **However**, **PEI decreases the time needed for nanoparticle uptake (Figure 4), due to the increased probability that cationic nanoparticles will interact with the anionic CM membrane, allowing for longer degradation in lysosomes.** In this thesis, the reacidification potential of nanoparticles **with and without PEI** surface modification was tested due to reported "proton-sink" effect of PEI within lysosomes [56].

Iterations in nanoparticle design tested whether or not increased cellular uptake due to PEI surface adsorption would restore pH dependent enzyme activity due to the summation of acidic nanoparticles in the lysosome and/or the optimized degradation rate of PLGA even while producing less initial proton release by mechanisms of PEI proton adsorption.

Nanoparticle surface modification and degradation rate for adequate cellular uptake and lysosomal reacidification respectively were key factors dependent on nanoparticle dosage and **treatment duration**. **Adequate cellular** uptake is defined by observed lysosomal colocalization with nanoparticles without nanoparticles outnumbering lysosomes. The dose of nanoparticles without PEI surface adsorption was increased to match the cellular uptake of nanoparticles with PEI adsorption for the same treatment period for best comparison of reacidification potential (see Figure 5). Nanoparticle doses were based on nanoparticles per cell by using the mass of nanoparticles over the surface area of cells (dose basis: CD = .00583333mg NP/cm^2 growth area). This has been reported to produce better/reproducible nanoparticle dosage results, since the uptake of nanoparticles is a stochastic mechanism that can be greatly influenced by volumes of treatment media [5, 57]. Nanoparticle diffusion through treatment media and sedimentation can influence the presentation of nanoparticles to the cell membrane.

To test uptake and acidification profiles, 8 and 24 hour pre-palmitate nanoparticle treatment periods were chosen. CM pre-palmitate treatment with nanoparticles allows the PLGA to degrade and establish pH control in the lysosome, since PLGA is inherently very slow to degrade [9]. Thus, short (8 hour) and long (24 hour) pre-palmitate treatment time periods were chosen to best determine the acidification potential of PLGA nanoparticles after a 4 hour treatment of 500uM palmitate.

It was observed that the addition of PEI to the surface of PLGA nanoparticles reduced the amount of time needed for **adequate nanoparticle uptake, where nanoparticles did not outnumber yet did colocalize with lysosomes**. Specifically, an 8 hour treatment of nanoparticles without PEI before palmitate treatment (cells imaged after 4 hour palmitate treatment) showed little uptake compared to those with PEI surface adsorption at the same

timepoint. However, a 24 hour pre-palmitate treatment with nanoparticles without PEI showed similar cellular uptake to that of nanoparticles with PEI surface adsorption at the same timepoint. Also, a 24 hour pre-palmitate treatment of nanoparticles with PEI surface adsorption showed little to no increase in cellular uptake over that of the 8 hour pre-palmitate treatment with the same nanoparticles. These observations are summarized in Figure 4, where the predicted cellular nanoparticle uptake duration of PLGA nanoparticles with and without PEI surface adsorption clearly demonstrates PEI dependent nanoparticle uptake kinetics.

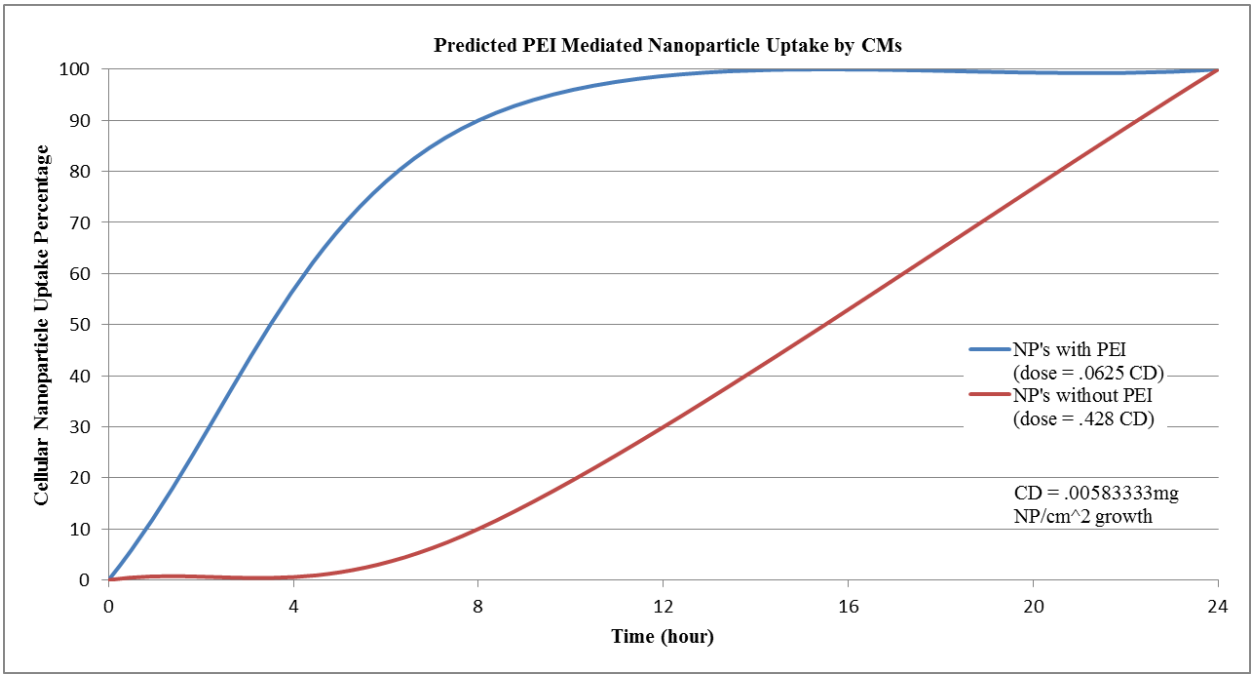

Figure 4: Predicted polyethylenimine (PEI) dictated nanoparticle uptake kinetics based on observations of 8 hour and 24 hour pre-palmitate nanoparticle uptake profiles.

Longer residence and subsequent more acid release within lysosomes, dictated by PEI mediated nanoparticle uptake, could result in reacidified and restored enzyme activity in lysosomes. PLGA degradation rate may also be increased upon longer residence within the lysosome, due to higher potential of acid-catalyzed hydrolysis within the acid lysosomal lumen. **Thus, nanoparticle treatment periods and surface coatings were tested to determine the acidification potential of these nanoparticles within lysosomes in the presence of acute lipotoxicity.**

In Figure 5, the cellular internalization and distribution mechanisms for modulating autophagy with PLGA nanoparticles is shown. Predicted intracellular events for the delivery of nanoparticles to lysosomes is depicted by the passage of nanoparticles from the extracellular space to endosomal, amphisomal, cytosolic or lysosomal compartments.

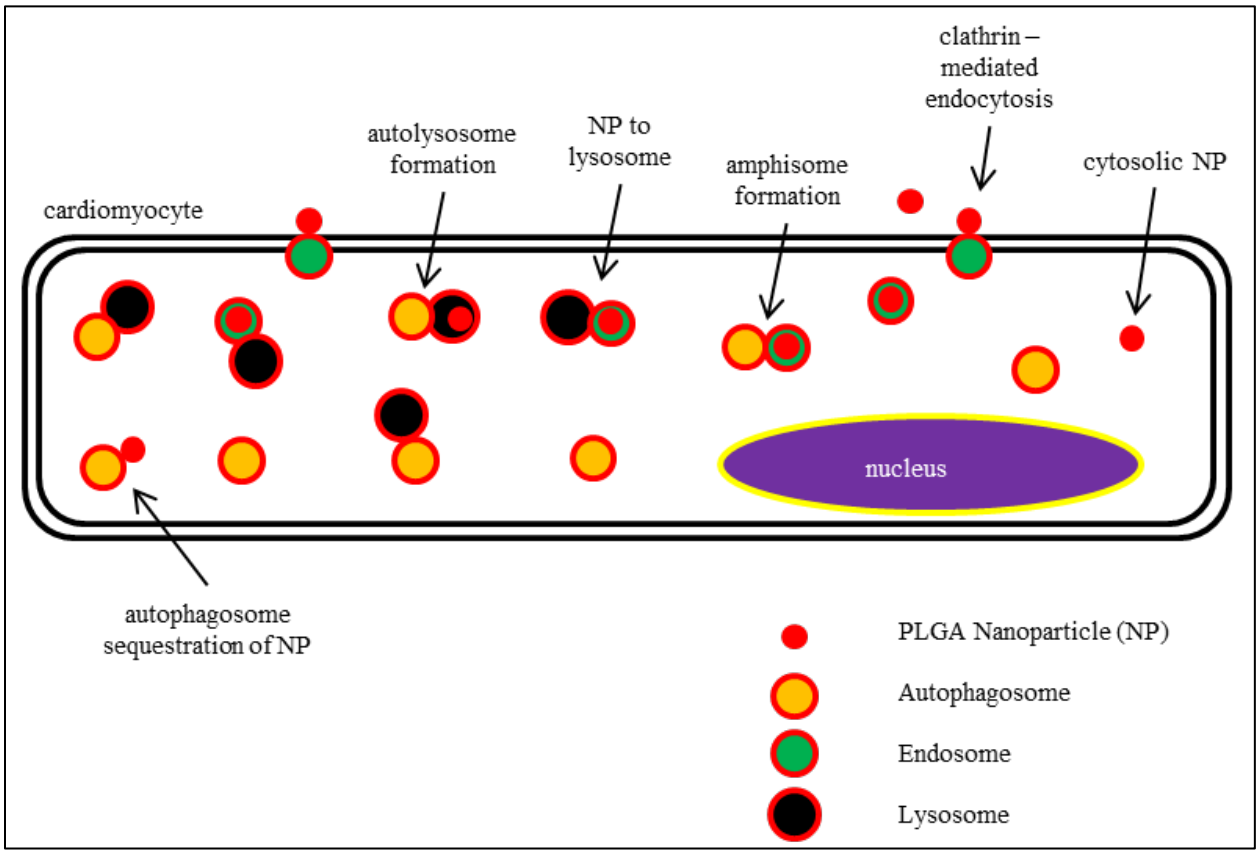

Figure 5: Diagram of cellular nanoparticle uptake and distribution to endosomes, amphisomes and lysosomes.

Specifically, the entry of PLGA nanoparticles into the endocytotic pathway by clathrin-mediated endocytosis and subsequent fusion with lysosomes or autophagosomes by lipid membrane curvature mechanisms produces nanoparticle loaded lysosomes and amphisomes respectively. Again, the lysosomal delivery of nanoparticles through the endocytosis pathway is well documented [6, 58], and is harnessed in this thesis as a **natural lysosome targeting delivery mechanism**.

Section V Results and Discussion

V.1 Lysosomal Deacidification

Lysosomal dysfunction resulting from lipotoxic conditions in differentiated H9c2 rat cardiomyoblasts (hereafter CMs) culture as reported by Jaishy *et al.* demonstrate that 4 hours of 500uM palmitate deacidified lysosomes and subsequently impaired enzyme activity and autophagic flux by blocking degradation of autophagosomes fused with lysosomes [3]. This lipotoxic effect is reversible as evidenced by the restored flux upon removal of palmitate. This acute effect of palmitate on lysosomal pH is the central question in this thesis. Figure 6 demonstrates the reproduction of this effect of lipotoxic concentrations of palmitate on CM lysosomal luminal pH.

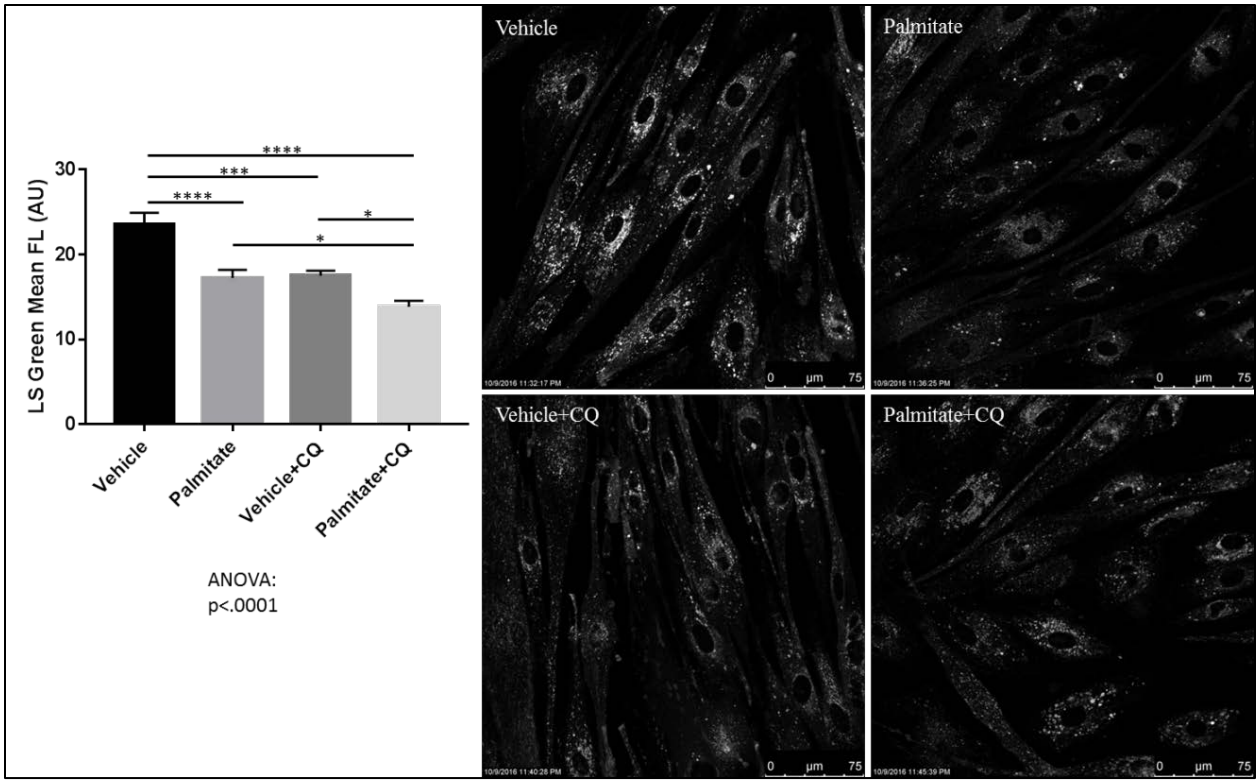

Figure 6: CM lysosomal luminal pH measurement after a 4 hour palmitate treatment with and without co-treatment of lysosomal deacidifying agent chloroquine (CQ). Graph of mean cellular fluorescence of LysoSensor Green live cell confocal imaging, with representative images. N's: Vehicle = 34, Palmitate = 57, Vehicle+CQ = 43, Palmitate+CQ = 44. Viable cells analyzed from two images from one experiment, and confirmed by additional experiments, data not shown. Error bars represent the standard error of the mean (SEM), which represents how well the mean is represented by the population, taking into account both standard deviation and sample size [59].

Chloroquine is a lysosomotropic small molecule with weak base properties that allow for its accumulation within lysosomes for subsequent increased luminal pH by unknown mechanisms [60]. Chloroquine has been used to treat malaria by causing lysosomal dysfunction by increasing lysosomal pH [61]. At low doses, chloroquine has been shown to impair autophagic flux and increase lysosomal pH in CMs [3]. Importantly, chloroquine's effect to block autophagosome degradation is not due to the inhibition of autophagosome fusion with lysosomes as seen with bafilomycin, a vATPase inhibitor. This was shown in CMs by increased GFP-LC3 labeled autophagosome colocalization with anti-Lamp1 antibody or LysoTracker stained lysosomes [3]. **As seen in Figure 6, palmitate reduces the pH in lysosomes to that of chloroquine treated cells, and further upon co-treatment with chloroquine, confirming palmitate induces lysosomal deacidification.**

V.2 Blocked Autophagic Flux

Autophagic flux is the movement of autophagosomes from formation to degradation through the cytosol of the CM. Various methods have been used to measure autophagic flux, and each should be carefully interpreted with the proper controls [62].

Cleaved and lipidated microtubule-associated protein 1 light chain 3 beta isoform II (LC3-II) is a marker of CM autophagosomes, whereby cytosolic LC3-I is cleaved and lipidated to autophagosomal membranes to enhance autophagosome formation and function. Sequestosome-1 (p62) acts as a delivery protein of ubiquitinated cargo, by binding autophagosome membrane bound LC3-II. These autophagosome marker proteins can be measured by Western blot to determine various states of autophagic flux when considered with the proper autophagic controls, such as chloroquine and rapamycin (RAP, an mTOR inhibitor to enhance autophagosome formation and flux) [62]. For example, increased degradation of these proteins indicates

increased autophagosome turnover in the presence of RAP. Glyceraldehyde-3-phosphate dehydrogenase (GAPDH) acts as a housekeeping protein unchanged by palmitate treatment to normalize autophagosome marker protein levels analyzed by Western blot.

To establish control conditions for the remainder of the experiments considering autophagic flux, CMs were treated with palmitate or vehicle with or without chloroquine (CQ), a lysosomotropic weak base known to deacidify lysosomes and inhibit lysosomal hydrolases. CQ blocks autophagic flux, by inhibiting the pH dependent degradation of autophagosomes. To determine if palmitate blocks autophagic flux, a co-treatment of CQ and palmitate can be compared to that of palmitate alone. Specifically, blocked autophagic flux can be observed if there is little to no increase in protein levels of autophagosome marker proteins p62 and LC3-II upon co-treatment of CQ and palmitate compared to that of palmitate alone [63]. Western blotting was performed from CM lysate to determine autophagosome marker proteins as described in Section VI.5.

In Figure 7, p62 levels are increased upon palmitate treatment and are similar to co-treatment with CQ. This indicates impaired p62 turnover, an indirect indicator of impaired autophagosome degradation. Additionally, LC3-II levels are similarly increased in palmitate and palmitate with CQ groups, **indicating impaired autophagosome degradation upon palmitate treatment in the acute lipotoxic conditions.**

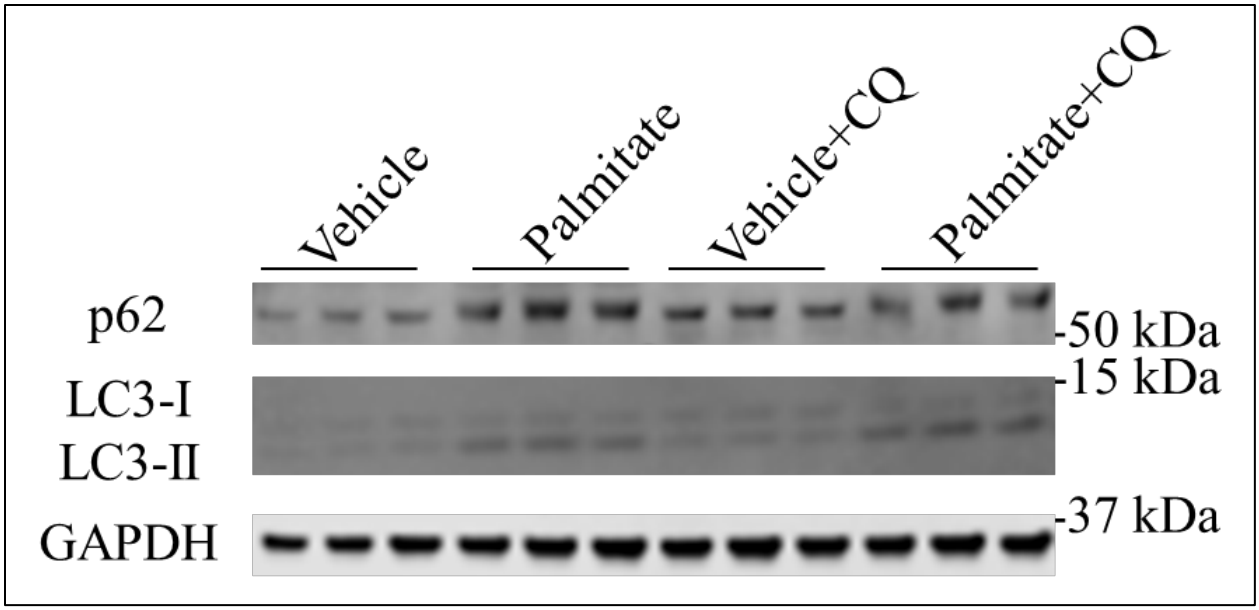

Figure 7: Western blot of autophagosome marker protein p62 and LC3-II levels with and without co-treatment of lysosomal deacidifying agent chloroquine (CQ). Images from the same membrane, with varied brightness and contrast settings for band visualization.

Co-treatment with RAP was performed to further delineate the increase in autophagosome marker protein levels from impaired degradation and enhanced production. In Figure 8, an increased cleavage of LC3-I to LC3-II is observed upon rapamycin treatment in conditions with palmitate treatment. This indicates that rapamycin can induce autophagosomal formation in the presence of palmitate, indicated by the increased cleavage of LC3-I. Interestingly, p62 levels decreased upon co-treatment of RAP with and without palmitate, indicating a possible increased degradation of p62 and increased autophagic flux in the presence of palmitate. These data in Figure 8 indicate that an increased autophagosome formation and possible increased autophagosome degradation paradigm is present when CMs are co-treated with lipotoxic concentrations of palmitate and RAP.

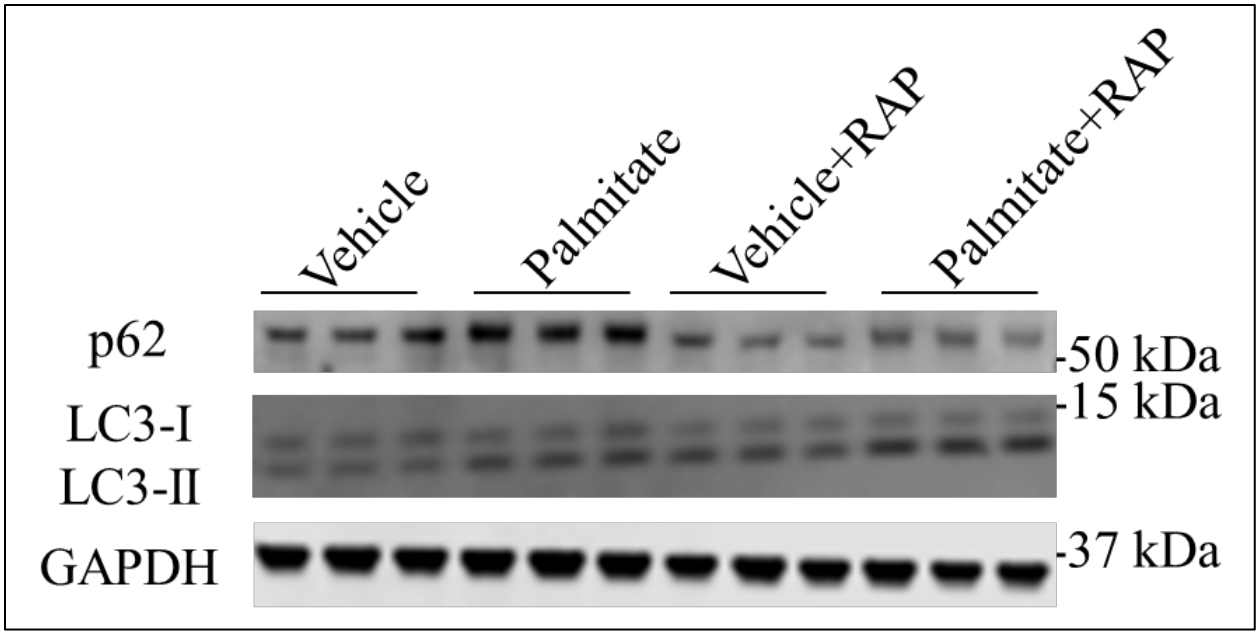

Figure 8: Western blot of autophagosome marker protein p62 and LC3-II levels with and without co-treatment of autophagic flux enhancer rapamycin (RAP). Images from the same membrane, with varied brightness and contrast settings for band visualization.

From these Western blot data, autophagosome turnover is impaired when CMs are treated with palmitate. To further define autophagic flux and not simply measure autophagosome marker protein levels, which can be influenced by additional cellular stresses and signals by delayed or increased transcription/translation, double tagged LC3 fluorescence was measured by confocal microscopy in live CMs. Fluorescent signals of the mCherry-GFP double tagged autophagosome marker protein indicate levels of increased or decreased autophagic flux. Specifically, upon formation of autophagosomes both the mCherry and GFP fluoresce and produce yellow puncta indicating an autophagosome. However, upon fusion with the lysosome GFP fluorescence is quenched by protonation leading to mCherry puncta. Thus, autophagosome passage and subsequent flux can be measured by analyzing GFP puncta in CMs. This experiment is also an indirect measure of lysosomal pH, since GFP fluorescence is dependent on pH.

In Figure 9, CMs co-treated with palmitate and CQ demonstrated similar data to that of autophagosome marker protein levels assessed by Western blot. Specifically, the number of cells with GFP puncta colocalized to mCherry puncta for both Palmitate+CQ and Palmitate groups were increased equivalently. **These data indicate acute lipotoxic cardiomyopathy modeled by palmitate treatment inhibits autophagic flux.** Interestingly, Vehicle+CQ images demonstrated trending yet non-significant increase in cells with GFP puncta colocalized with mCherry puncta over that of Vehicle images. This is most likely due to a lower number of images analyzed for Vehicle in this experiment. Increasing the number of images analyzed for Vehicle would indicate significant increases in cells with GFP-mCherry colocalized puncta in Vehicle+CQ over that of Vehicle, since error bars do not overlap in these data.

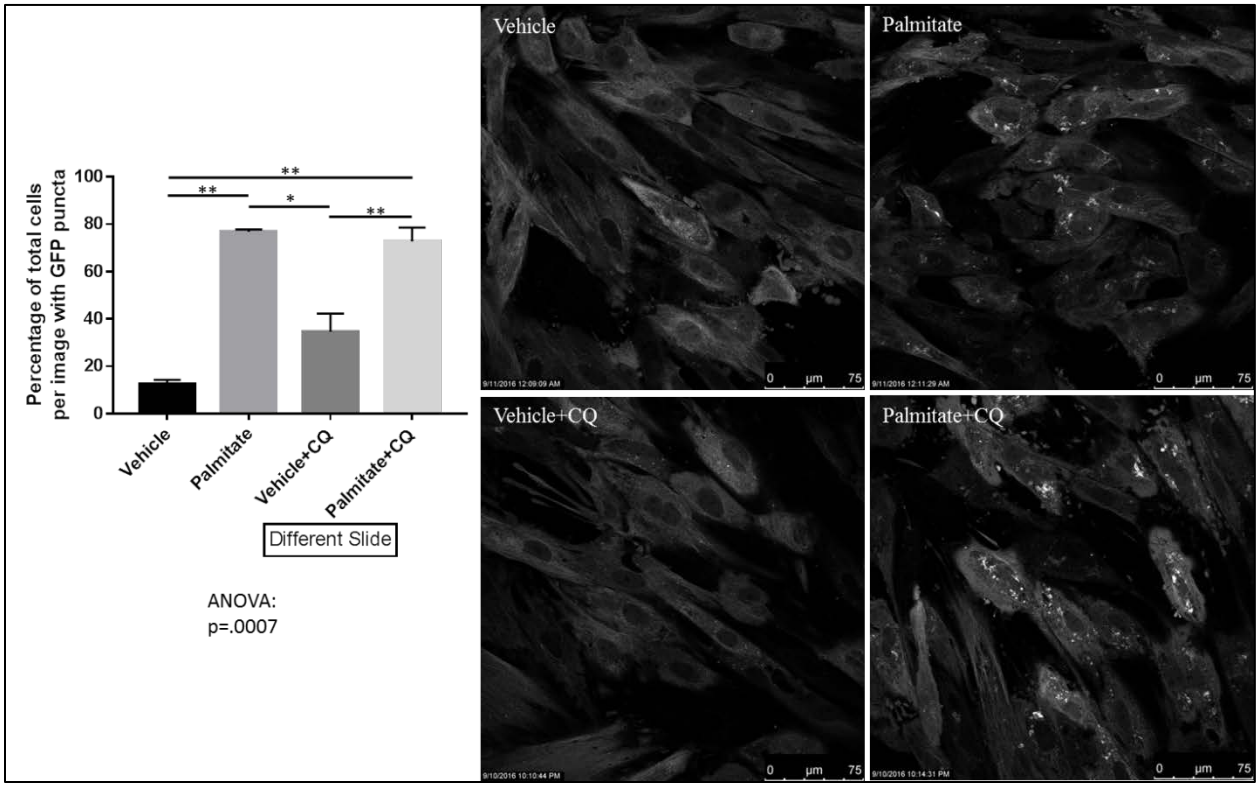

Figure 9: Autophagic flux assessment of palmitate and chloroquine control conditions by confocal fluorescent imaging of mCherry-GFP-LC3 retroviral expression in live CMs. GFP puncta quantification and representative images. Graph represents percentage of total cells per image that have colocalized GFP puncta with that of mCherry. Two images for Vehicle and Palmitate groups and four images for Vehicle+CQ and Palmitate+CQ groups were analyzed from **one** experiment. Error bars indicate SEM.

These control experiments replicate palmitate-induced lysosomal deacidification and subsequent inhibited autophagic flux in an acute lipotoxic model, as previously reported [3].

V.3 PLGA Nanoparticle Characteristics

As described in Section IV.2, nanoparticles were designed with theoretically optimal acid release (degradation rate) and are well positioned for testing of acidification potential in lysosomes upon adequate CM uptake. In addition to these optimizations, several iterations of nanoparticle design discussed below were used to determine the characteristics of nanoparticles shown in Table 2, which are used for the remainder of lysosomal reacidification, enzyme activity and autophagic flux restoration experiments.

Table 2: PLGA nanoparticle characteristics measured by a dynamic light scattering. Standard deviation (SD).

Nanoparticle Formulation	Diameter (z-average)	Polydispersity Index	Surface Charge (zeta-potential)
PLGA +PEI + free glycolic acid	222.3nm (SD 64.48nm)	.058	+35.1mV (SD 5.80mV)
PLGA - PEI + free glycolic acid	177.6nm (SD 43.54nm)	.036	-47.3 mV (SD 7.18mV)

Briefly, nanoparticle size, polydispersity and surface charge played major roles in nanoparticle uptake in CMs due to nanoparticle aggregation and cell membrane interactions. Additionally, nanoparticle dose and treatment times were varied as described in Section IV.2 to achieve desired uptake at the time of measurement of lysosomal pH, enzyme activity and autophagic flux.

A fluorescent autophagosome labeling kit (Cyto-ID, Enzo) was used investigate the effect of aggregation and size on autophagosome formation in cultured CMs. Cyto-ID, a selective proprietary autophagosome fluorescent label shown to highly colocalize with RFP-LC3 in HeLa cells [64] is not quenched upon lysosome fusion (even though colocalization with lysosomal probes was minimal). Thus, this fluorescent probe allowed the visualization of autophagosome like structures, yet cannot be interpreted as an autophagic flux assay. Preliminary iterations of nanoparticle design indicated larger particles and or aggregates colocalized with the Cyto-ID

probe, indicating that the aggregation/size of the nanoparticles induced autophagosome formation, or produced large vesicles that were labeled by Cyto-ID (Figure 10).

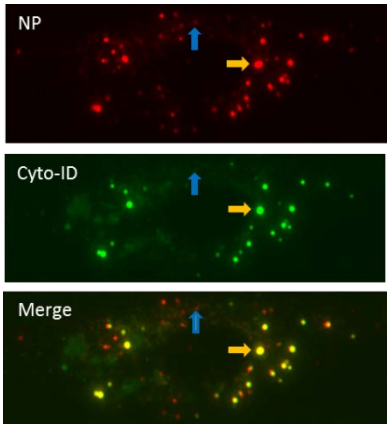

Figure 10: Cyto-ID labeled structures show increased labeling with larger nanoparticles (NPs). Orange arrow indicates larger nanoparticle, blue arrow indicates smaller nanoparticle. This is a single cell from epifluorescence images of live CMs treated in palmitate.

This evidence was taken as a precaution in assuming that any acidic nanoparticle size could influence lysosome-autophagy function, but in fact could induce formation of autophagosome/amphisomal vesicles that subsequently produce cellular stress. Subsequent design of the nanoparticle with PEI surface adsorption consisted of size and polydispersity reduction to ~220nm and .03 respectively (Table 2). Since lysosomes are on average 500nm in diameter, this size was adequate to produce colocalization with lysosomes without disrupting lysosomal biology and without inducing large autophagosome/amphisomal structures as seen with subsequent results.

In parallel with size reduction, PLGA nanoparticles were modified to obtain a **positive** surface charge, as measured by the zeta-potential of particles. It has been shown that a positive surface charge decreases nanoparticle uptake duration due to the favorable electrostatic interaction with the negative cell membrane [55]. Thus, polycations polylysine and polyethylenimine were surface adsorbed to the carboxylate (net negative) surface of the PLGA nanoparticle. Polylysine (PLL) demonstrated a flip of nanoparticle nascent surface charge of -40 mV to +10mV.

However, due to high variability of PLL treatment where similar treatment conditions **did not** yield reproducible or reliable results as well as producing a dramatic increase in polydispersity index, PLL **was not pursued**. Branched polyethylenimine (PEI) was pursed as an alternative (and much cheaper) method to flip negative to positive nanoparticle surface charge. PEI treatments consistently yielded a -40mV to +35mV nanoparticle surface charge flip.

Combining both PEI and size reduction, the polydispersity index was greatly reduced from as great as .8 to .03. Optimized methods of single emulsion solvent evaporation/extraction nanoparticle formulation produced a consistent polydispersity index of about .03. Nanoparticle diameter measured by dynamic light scattering increased about 40nm when PEI was adsorbed to the surface for charge modification. This yielded a PEI modified nanoparticle diameter of ~220nm from an unmodified PLGA nanoparticle diameter of ~180nm (Table 2).

In parallel with size reduction and surface modification for optimal cellular uptake, PLGA polymer characteristics were **designed** for rapid degradation on the timescale of adequate reacidification measured at 8 and 24 hours pre-palmitate nanoparticle treatments as **discussed in Section IV.2**. Briefly, PLGA degrades more quickly with reduction in molecular weight, a measure of polymer length, and an approach to a 50:50 ratio of DL lactide to glycolide. Reduced PLGA molecular weight indicates shorter chains of polymer in the formulation, which upon hydrolysis, more easily escape the nanoparticle than longer chains and also take less time to fully degrade in to acidic monomers. Initial testing of 50:50 PLGA consisted of a higher molecular weight PLGA (~50kDa) with results demonstrating little to no acidification (data not shown). Thus, the lowest bound available of PLGA molecular weight (4.6kDa) was used as the basis of reacidification for the remaining experiments.

Free DL lactide **polymer** (PLA) was incorporated into the PLGA polymer upon formulation of nanoparticles to see if the disruption of PLGA polymer by DL lactide would increase degradation and subsequent acid release. However, this strategy was abandoned due to clarification on the increased PLGA crystallinity with PLA, which theoretically reduces degradation rate. **Rather**, free non-polymer glycolic acid was incorporated into the PLGA nanoparticle formulation to increase acid release by free glycolic acid escape from the nanoparticle, and increasing nanoparticle porosity thought to enhance PLGA bulk degradation by allowing increased surface area for hydrolysis. Local concentrations of free glycolic acid within the nanoparticle can also accelerate acid catalyzed hydrolysis of the nanoparticle, as discussed in Section IV.2.

Two pre-palmitate treatment periods of 8 hours and 24 hours for nanoparticles with PEI and one pre-palmitate treatment period of 24 hours for nanoparticles without PEI were utilized for the remainder of the data due to the observed nanoparticle uptake kinetics (Figure 4). This was performed to test PEI's effect on acidification potential and nanoparticle uptake as discussed in Section IV.2. The 8 hour pre-palmitate timepoint for nanoparticles without PEI was **not utilized** due to very low nanoparticle uptake utilizing the same dose as 24 hour pre-palmitate treatment (Figure 4). The 24 hour pre-palmitate treatment dose for nanoparticles without PEI (.428 CD, where CD = .0053333mg NP/cm^2 cell culture) produced nanoparticle uptake similar to that of the dose of nanoparticles with PEI (.0625 CD) at both 8 hour and 24 hour pre-palmitate treatment times. Thus, a shorter incubation period of nanoparticles with PEI surface adsorption demonstrated rapid and adequate uptake compared to that of unlabeled nanoparticles (Figure 4). **As seen in Figures 11-13, the three-dimensional rendering of z-stack images of nanoparticle treated CMs in the presence of palmitate with LysoTracker Blue and LysoLive phosphatase activity probes demonstrate high nanoparticle colocalization with both probes.**

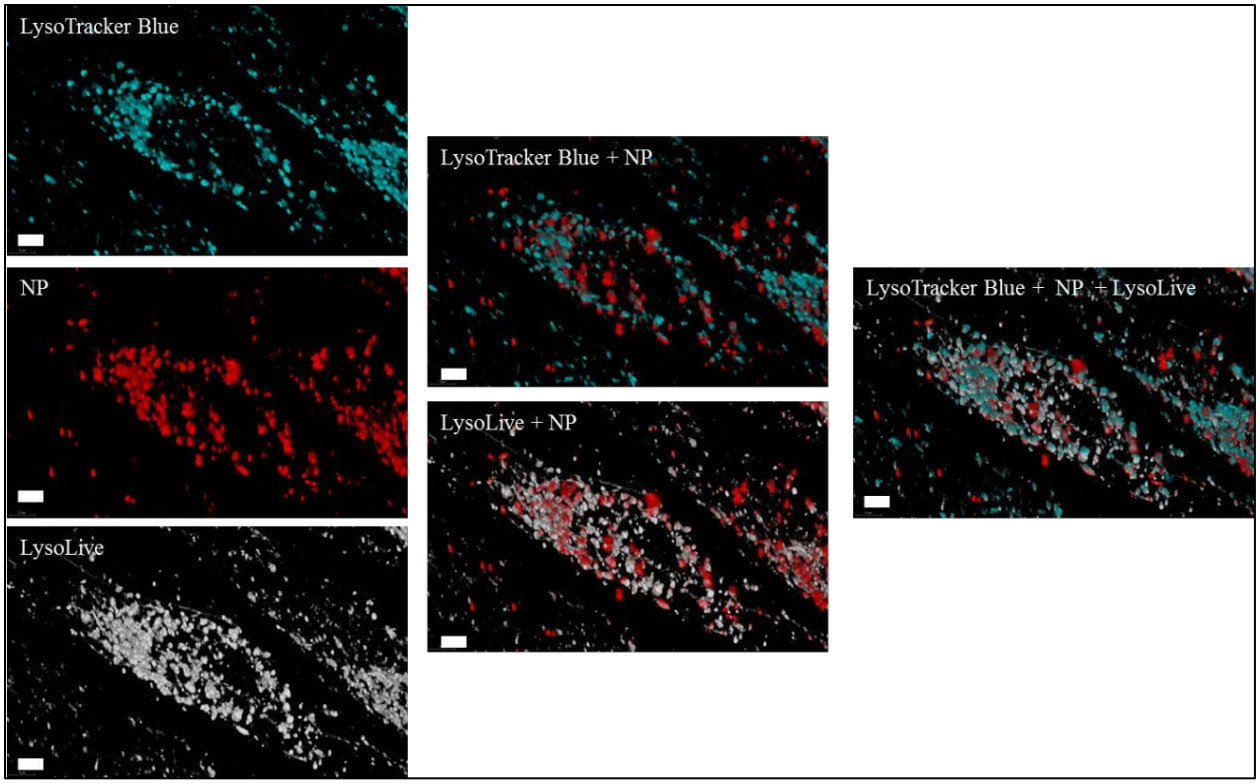

Figure 11: Three dimensional reconstruction of confocal z-stack images of live CMs after palmitate treatment with prior **8 hour pre-palmitate nanoparticle (NP) with PEI** treatment. Scale bar 5um.

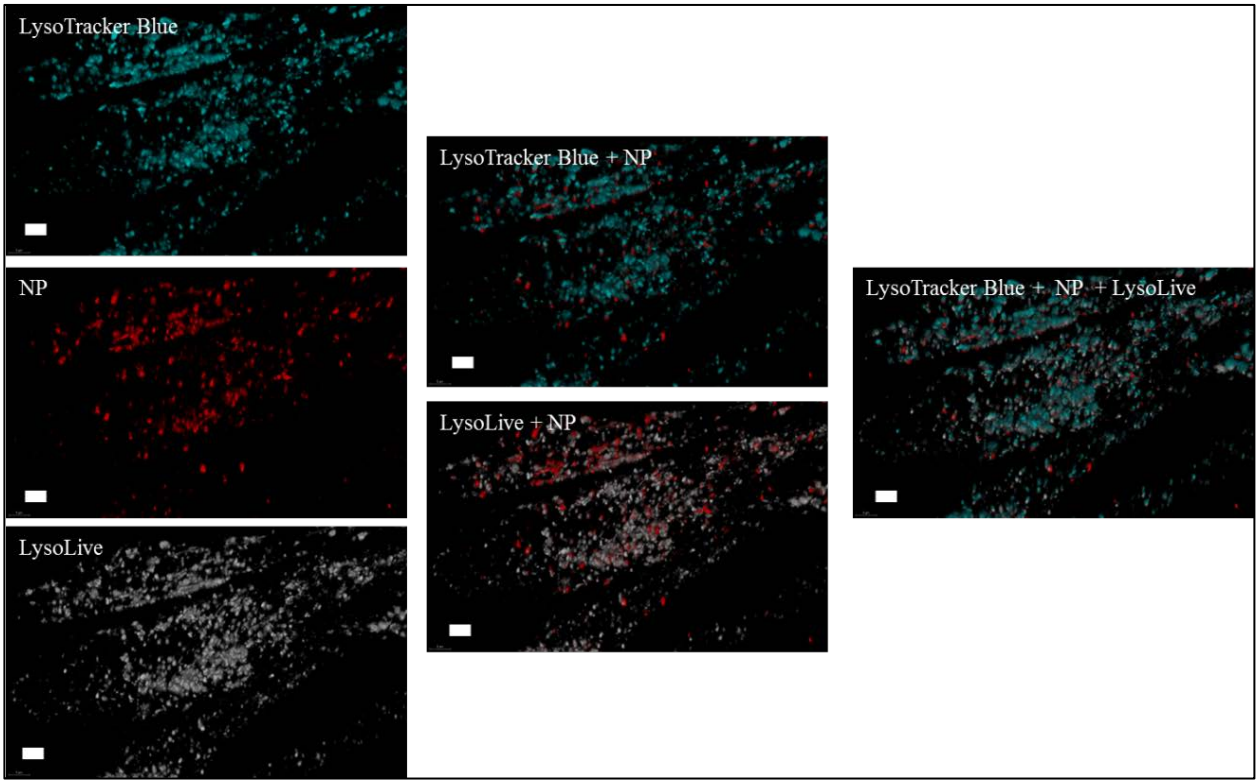

Figure 12: Three dimensional reconstruction of confocal z-stack images of live CMs after palmitate treatment with prior **24 hour pre-palmitate nanoparticle (NP) with PEI** treatment. Scale bar 5um.

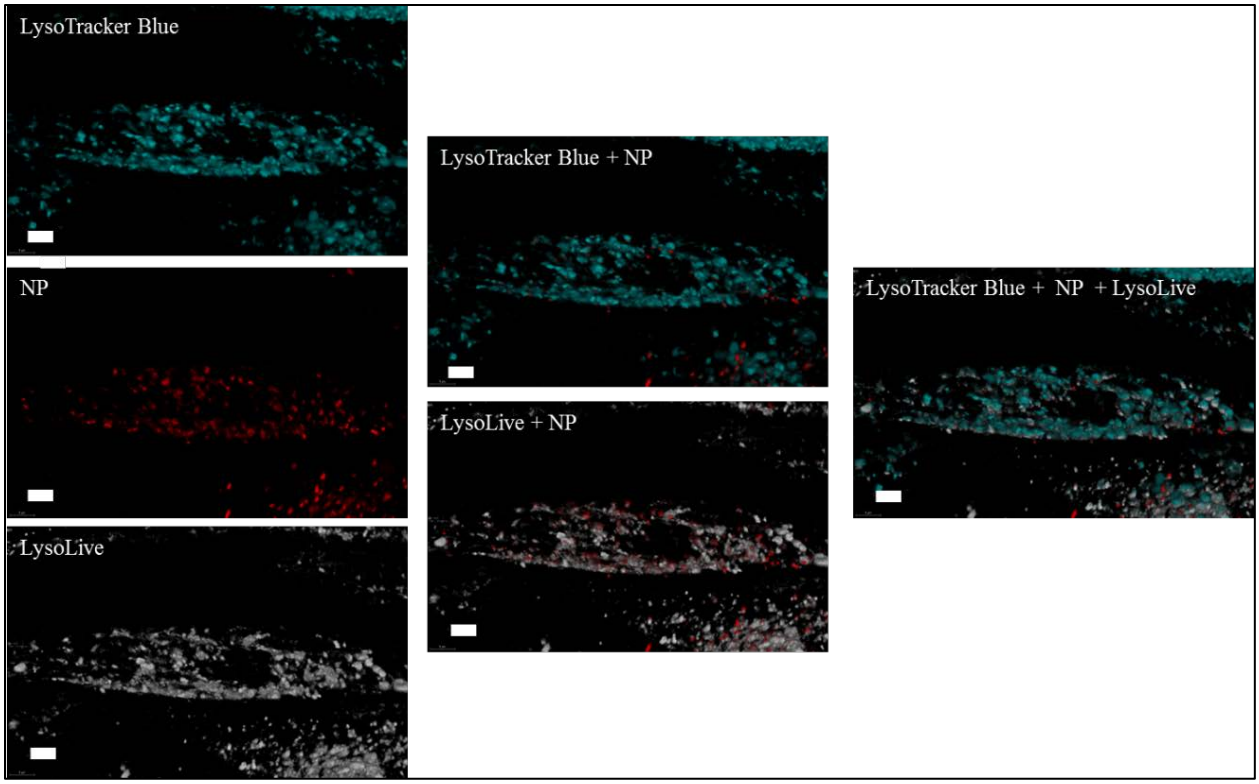

Figure 13: Three dimensional reconstruction of confocal z-stack images of live CMs after palmitate treatment with prior **24 hour pre-palmitate nanoparticle (NP) without PEI** treatment. Scale bar 5um.

These results indicate that the nanoparticles with characteristics in Table 2 for short and long treatment periods pre-palmitate, can traffic to CM lysosomes (labeled with LysoTracker Blue) where a lysosomal enzyme activity probe is also present (LysoLive). Although not quantified directly, observations over the field of view indicate that CMs with internalized nanoparticles contained a high portion of nanoparticles colocalized with lysosomes. There was a portion of nanoparticles **not** colocalized with lysosomes, possibly remaining in the cytosol or internalized by other organelles or vesicles, such as mitochondria or autophagosomes (Figure 5).

V.4 Restoration of Lysosomal pH by PLGA Nanoparticles

Lysosomal reacidification by nanoparticles was tested for nanoparticles with and without PEI surface adsorption to determine the best balance in PEI dictated nanoparticle uptake and

reacidification. Specifically, the proton-sink effect of PEI is thought to inhibit lysosomal reacidification, by amine groups binding protons released from degrading PLGA. However, PEI surface adsorption to the nanoparticle **decreases** cellular uptake duration due to cationic interactions with the anionic cell membrane and thereby could increase acidification potential described earlier. Thus, pre-palmitate treatment times were varied to test time for reacidification dependent on PEI dictated nanoparticle uptake.

Lysosomal pH change upon an 8 hour pre-palmitate treatment of PLGA nanoparticles with PEI is shown in Figure 14, with increased fluorescence indicating decreased lysosomal pH.

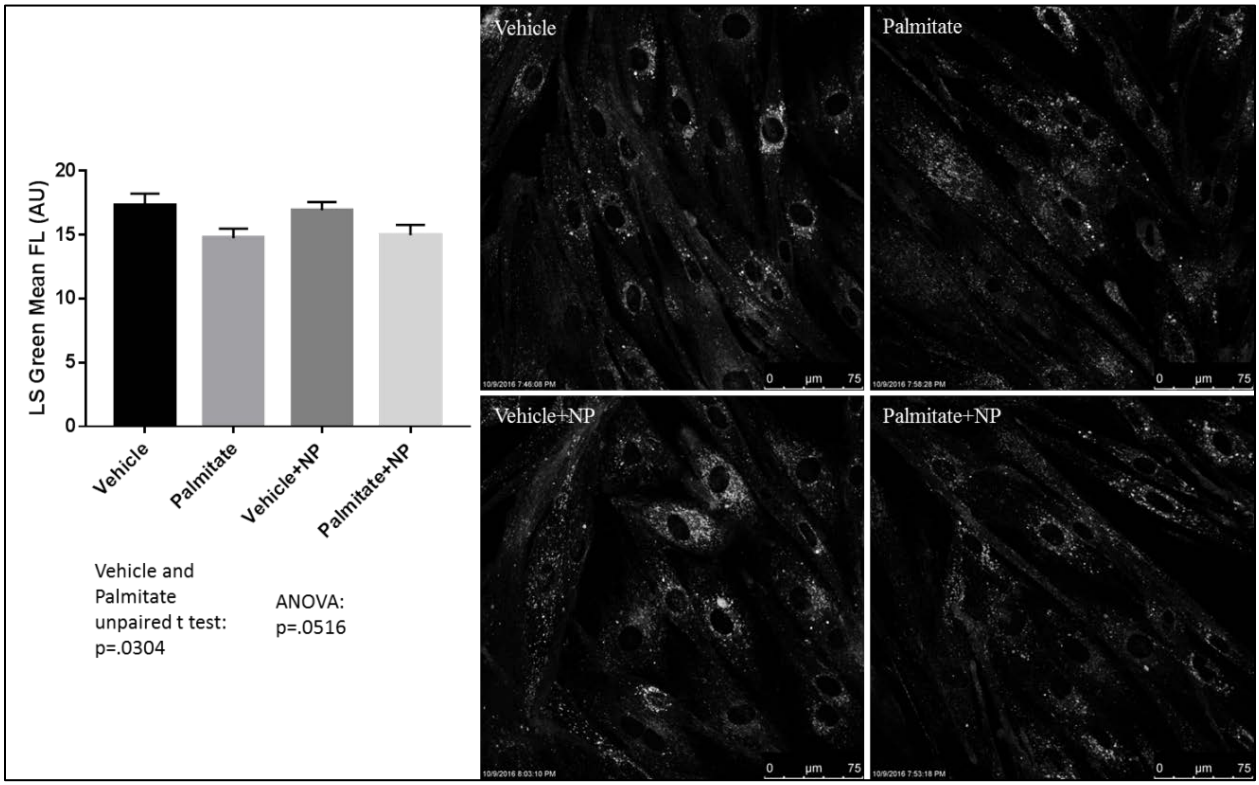

Figure 14: CM lysosomal luminal pH measurement after a 4 hour palmitate treatment with a prior **8 hour pre-palmitate treatment of PLGA nanoparticles with surface adsorbed PEI**. Graph of mean cellular fluorescence of LysoSensor Green live cell confocal imaging, with representative images. N's: Vehicle = 70, Palmitate = 56, Vehicle+NP = 30, Palmitate+NP = 36. Viable cells analyzed from three images from one experiment, and confirmed by additional experiments, data not shown. Cells with internalized nanoparticles only analyzed in NP treatment groups. Error bars represent the standard error of the mean (SEM), which represents how well the mean is represented by the population, taking into account both sample standard deviation and sample size [59].

These data indicate that **an 8 hour pre-palmitate treatment with nanoparticles with PEI on their surface is not adequate to reacidify lysosomes upon an acute palmitate challenge.** Iterations of this experiment showed variance in the reacidification profile for this treatment regime, and thus point to a possible sensitivity issue regarding the method to measure lysosomal pH change. As described in Section VI.1, methods to accurately determine small changes in pH from degrading PLGA nanoparticles ranged from plate reading, flow cytometry and confocal imaging of multiple commercially available probes. LysoSensor Green measurement was the only method whereby equipment at the University of Iowa could reproducibly measure a change in lysosomal pH. The dynamic range of this pH sensor is confirmed upon lysosomotropic chloroquine treatment, as seen earlier in Figure 6. **However, small changes in pH from degrading PLGA nanoparticles with PEI demonstrated variable and non-significant restoration in lysosomal pH upon an 8 hour pre-palmitate treatment.**

To test whether or not the nanoparticles would produce acidification upon longer pre-palmitate treatment, CMs were treated for 24 hours with nanoparticles containing PEI surface adsorption. **Longer pre-palmitate treatment of nanoparticles with surface adsorbed PEI demonstrated a significant restoration in pH after palmitate**, as shown in Figure 15. This indicated that PEI surface adsorbed nanoparticles could indeed restore proton concentrations within lysosomes with impaired vATPases. These data also indicate that the proton-sink effect of PEI was overcome by a longer pre-palmitate treatment. This indicates that the proton adsorption of PEI became saturated and/or a longer treatment period increased the rate of PLGA hydrolysis and acid release by the previously described Fickian behavior of increased degradation from decreasing molecular weight as polymer chains are cleaved [52]. **Thus, longer nanoparticle treatment before the addition of palmitate may increase the rate at which acidic**

monomers are released from PLGA, subsequently reacidifying lysosomal lumen even in the presence of PEI and inhibited vATPases.

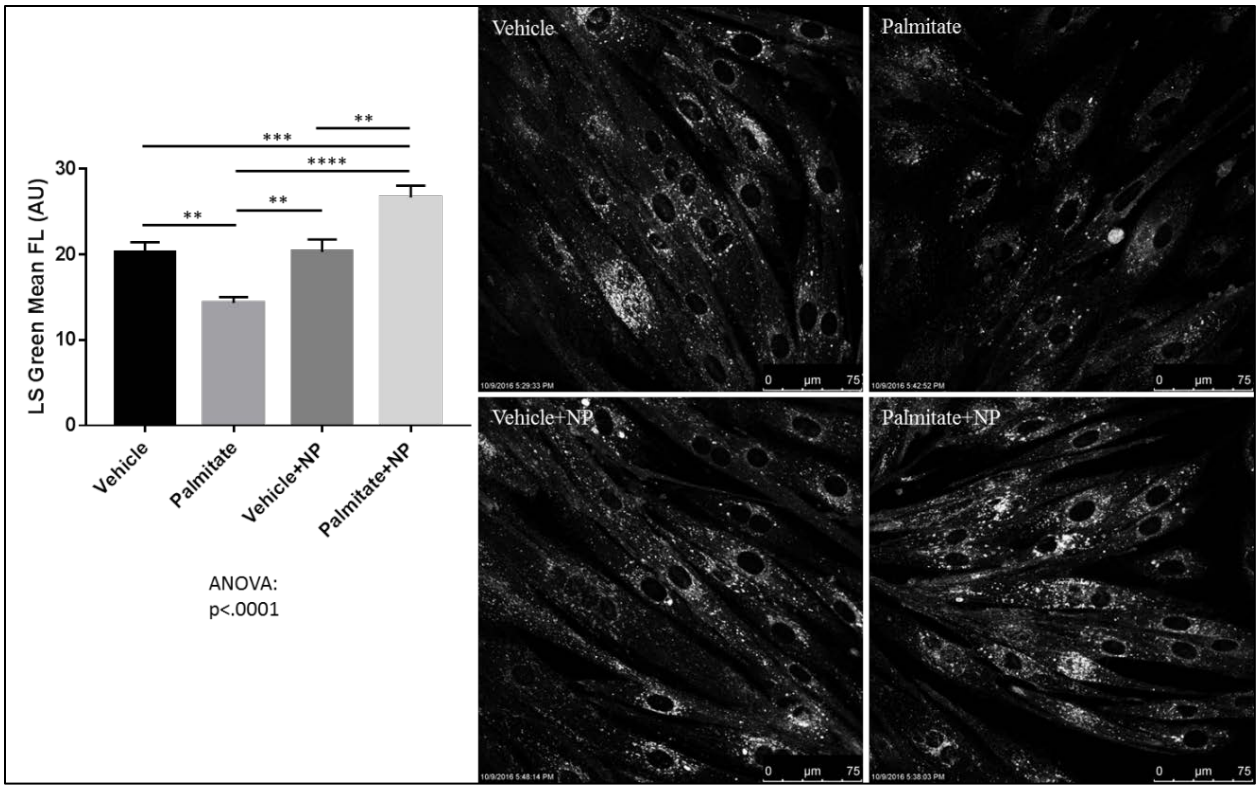

Figure 15: CM lysosomal luminal pH measurement after a 4 hour palmitate treatment with a prior **24 hour pre-palmitate treatment of PLGA nanoparticles with surface adsorbed PEI**. Graph of mean cellular fluorescence of LysoSensor Green live cell confocal imaging, with representative images. N's: Vehicle = 42, Palmitate = 41, Vehicle+NP = 36, Palmitate+NP = 45. Viable cells analyzed from two images from one experiment, and confirmed by additional experiments, data not shown. Cells with internalized nanoparticles only analyzed in NP treatment groups. Error bars represent the standard error of the mean (SEM).

To further test the effect of PEI on PLGA nanoparticle acidification potential, CMs were treated for 24 hours with nanoparticles **without** PEI prior to palmitate treatment. The 8 hour pre-palmitate treatment duration for these non-PEI nanoparticles was not pursued due to observations of very low nanoparticle uptake and distribution at higher doses (Figure 4). Additionally, the dose of these non-PEI nanoparticles was increased relative to PEI coated nanoparticles to match intracellular distribution at the time of lysosomal pH measurement, as depicted in Figure 4.

CMs with internalized PLGA nanoparticles without surface adsorbed PEI did not significantly decrease pH in the presence of palmitate as shown in Figure 16. Additionally, an unpaired t test between palmitate and palmitate with nanoparticle treated CMs indicated a p value of .0592. Nanoparticles without PEI surface adsorption **did** show cellular uptake equivalent to that of CMs nanoparticles with PEI, but in fewer cells and at a higher incubation dosage. These data indicate that the shorter time observed for adequate nanoparticle uptake when PEI is surface adsorbed to nanoparticles increases the time of degradation inside lysosomes, and subsequently increases acidification potential over that of nanoparticles that do not have PEI.

Additionally, the **distribution** of nanoparticles within the CM to lysosomes was observed to be higher with PEI treated nanoparticles in this timepoint (data not shown). This indicates that high nanoparticle cellular distribution may favorably decrease pH in the period measured to produce a significant change in lysosomal pH upon palmitate treatment. **However**, the trending decrease in pH from nanoparticles without PEI surface adsorption at 24 hour pre-palmitate incubation indicates **longer incubation may produce a more substantial change in pH**.

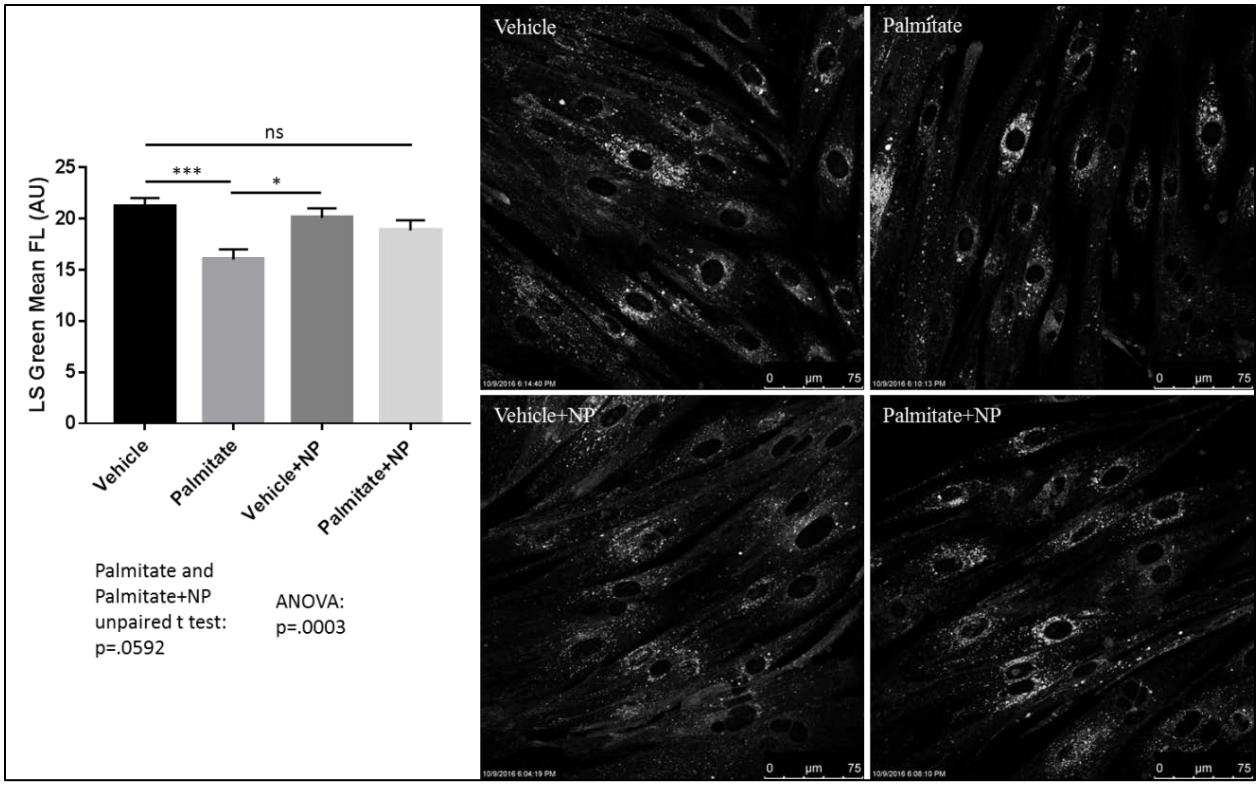

Figure 16: CM lysosomal luminal pH measurement after a 4 hour palmitate treatment with a prior **24 hour pre-palmitate treatment of PLGA nanoparticles without surface adsorbed PEI**. Graph of mean cellular fluorescence of LysoSensor Green live cell confocal imaging, with representative images. N's: Vehicle = 56, Palmitate = 48, Vehicle+NP = 34, Palmitate+NP = 28. Viable cells analyzed from two images from one experiment, and confirmed by additional experiments, data not shown. Cells with internalized nanoparticles only analyzed in NP treatment groups. Error bars represent the standard error of the mean (SEM).

Interestingly, lysosomal size was increased upon palmitate treatment quantified by LysoTracker Blue probes (data not shown). This is in agreement with the lipotoxic phenotype of dysfunctional lysosomes, where autophagosome-lysosome fusion is not inhibited, so subsequent size of lysosomes/autolysosomes is larger than normal. This result is an interesting finding from the multiple parallel fluorescent experiments, where LysoTracker Blue was measured in parallel with LysoSensor Green in efforts to normalize concentration variable LysoSensor Green intensities [65]. Normalization was not performed due to the pH modulation of LysoTracker Blue in CQ treatments, previously reported to independent of pH.

V.5 Restoration of Lysosomal Enzyme Activity by PLGA Nanoparticles

Decreased hydrolase activity within CM lysosomes after treatment of palmitate for 4 hours has been reported [3] and is reproduced in this section. As discussed earlier, lysosomal degradative enzymes are highly pH controlled, with increases in pH inactivating their catalytic activity through deprotonation of catalytic active sites. To test whether PLGA nanoparticles could restore lysosomal enzymatic activity, identical nanoparticle types and treatment times as that of lysosomal pH measurement were tested for lysosomal phosphatase activity. Decreased enzymatic activity upon palmitate treatment was reproduced in each of these nanoparticle experiments.

For an 8 hour pre-palmitate nanoparticle treatment with PEI surface adsorption, phosphatase activity was significantly restored in the presence of palmitate challenge (Figure 17). These results indicate that the small changes in pH not detected by available pH measurements in live CMs were significant enough to produce a restored biological function. The immediate microenvironment around degrading PLGA nanoparticles could have an adequate reduction in pH, whereby phosphatase activity is increased upon protonation.

In addition to phosphatase activity, cathepsin L activity was measured for these nanoparticles (Figure 18). Results indicate a **significant increase in cathepsin L enzymatic activity** as demonstrated by increased cleavage of a fluorogenic probe targeted to cathepsin L by bi-substitution of two copies of phenylalanine-arginine. Cleavage these target sequences frees a bound cresyl violet fluorophore and subsequently produces light when excited. Increased fluorescence also indicates increased substrate cleavage and enzyme activity for the phosphatase activity probe.

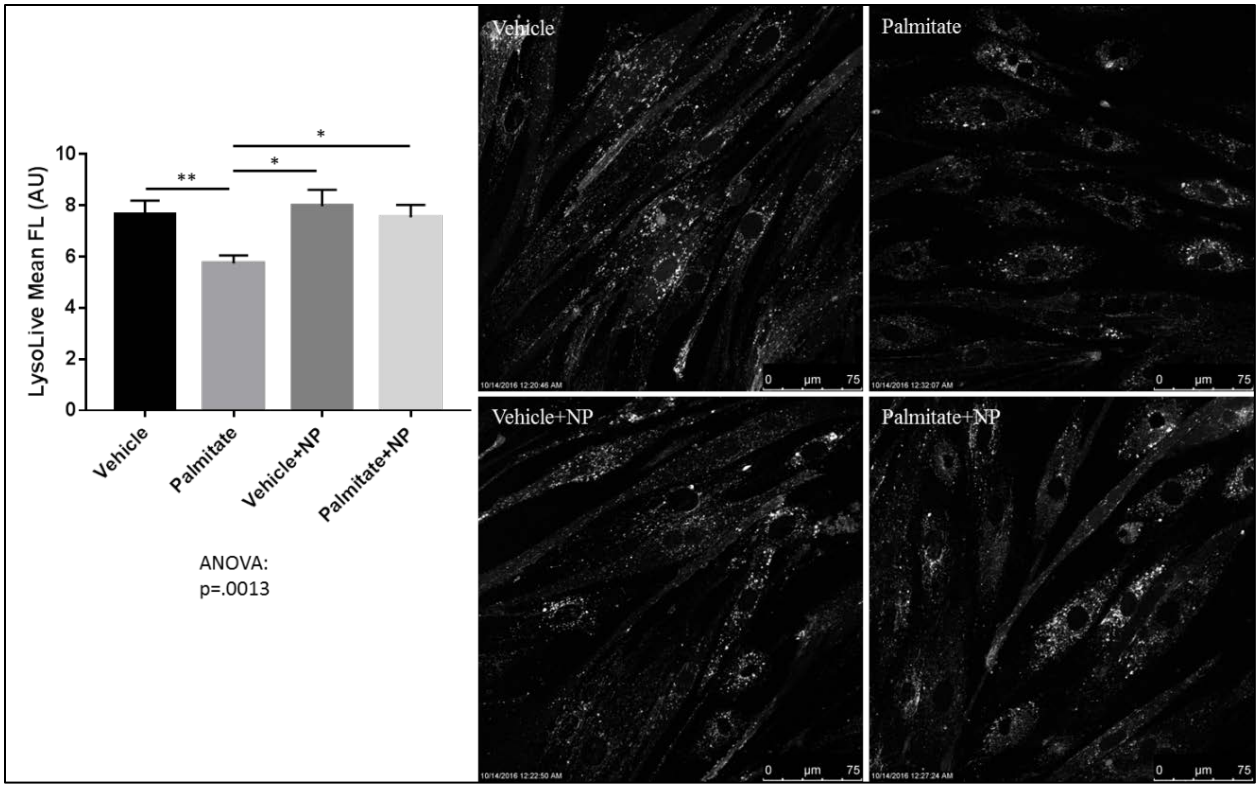

Figure 17: CM lysosomal phosphatase activity measurement after a 4 hour palmitate treatment with a prior **8 hour pre-palmitate treatment of PLGA nanoparticles with surface adsorbed PEI**. Graph of mean cellular fluorescence of LysoLive live cell confocal imaging, with representative images. Viable cells analyzed from two images from one experiment. N's: Vehicle = 42, Palmitate = 55, Vehicle+NP = 22, Palmitate+NP = 35. Cells with internalized nanoparticles (NPs) only analyzed in NP treatment groups. Error bars indicate SEM.

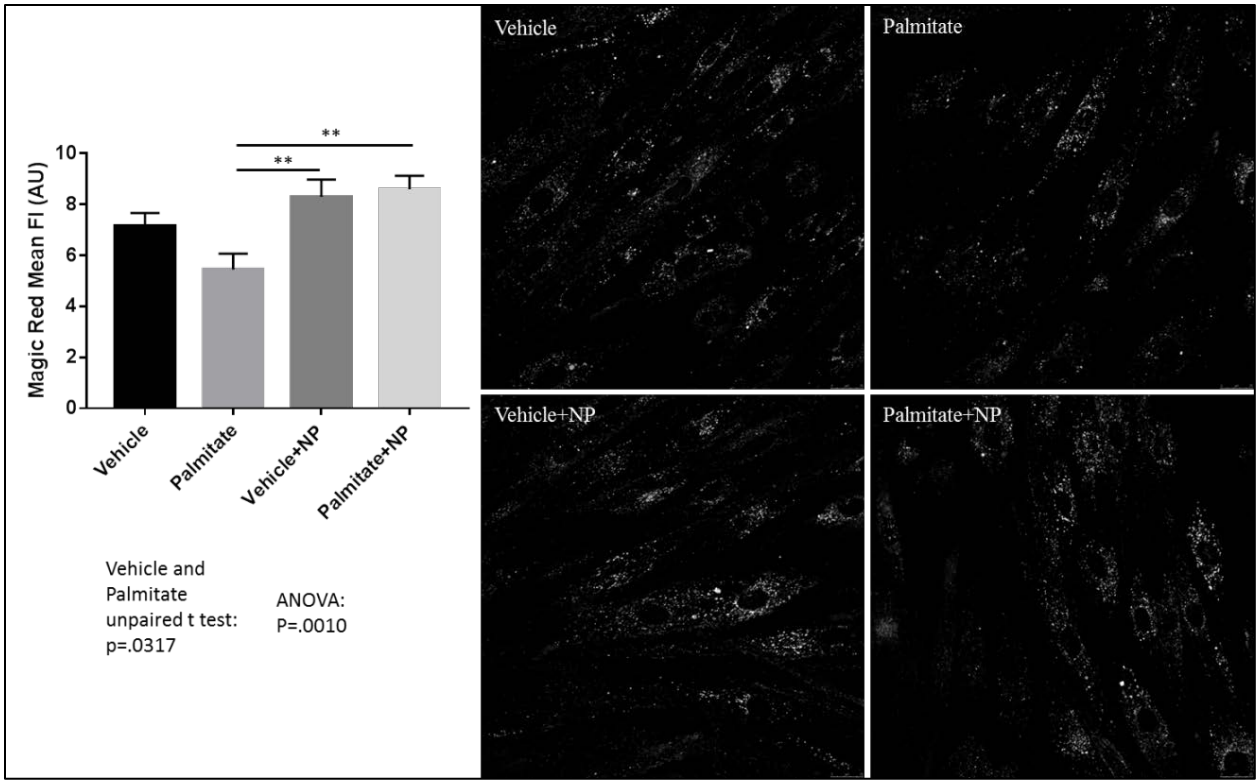

Figure 18: CM lysosomal cathepsin L activity measurement after a 4 hour palmitate treatment with a prior **8 hour pre-palmitate treatment of PLGA nanoparticles with surface adsorbed PEI**. Graph of mean cellular fluorescence of Magic Red live cell confocal imaging, with representative images. All viable cells in each group analyzed from three images from one experiment. N's: Vehicle = 71, Palmitate = 50, Vehicle+NP = 57, Palmitate+NP = 76. Error bars indicate SEM.

As with measurement of lysosomal pH, longer pre-palmitate incubation with nanoparticles were tested for changes in lysosomal enzyme activity to determine if increased time for PLGA degradation increased acid release and subsequent enzyme activity in lysosomes. **For a 24 hour pre-palmitate treatment of PEI surface adsorbed nanoparticles, PLGA nanoparticle treatment significantly increased phosphatase activity the presence of palmitate challenge over that of palmitate by an unpaired t test (Figure 19).** However, this was not significant upon ANOVA analysis.

Upon analysis of these data, CMs treated with vehicle with prior nanoparticle treatment did indicate an impaired phosphatase activity. However, upon palmitate challenge, this effect was not observed. PEI could play a role in this observed effect; however, this result was not pursued

due to evidence that with an 8 hour pre-palmitate treatment, nanoparticles with PEI restored enzyme activity in the presence of palmitate and did not affect enzyme activity in vehicle.

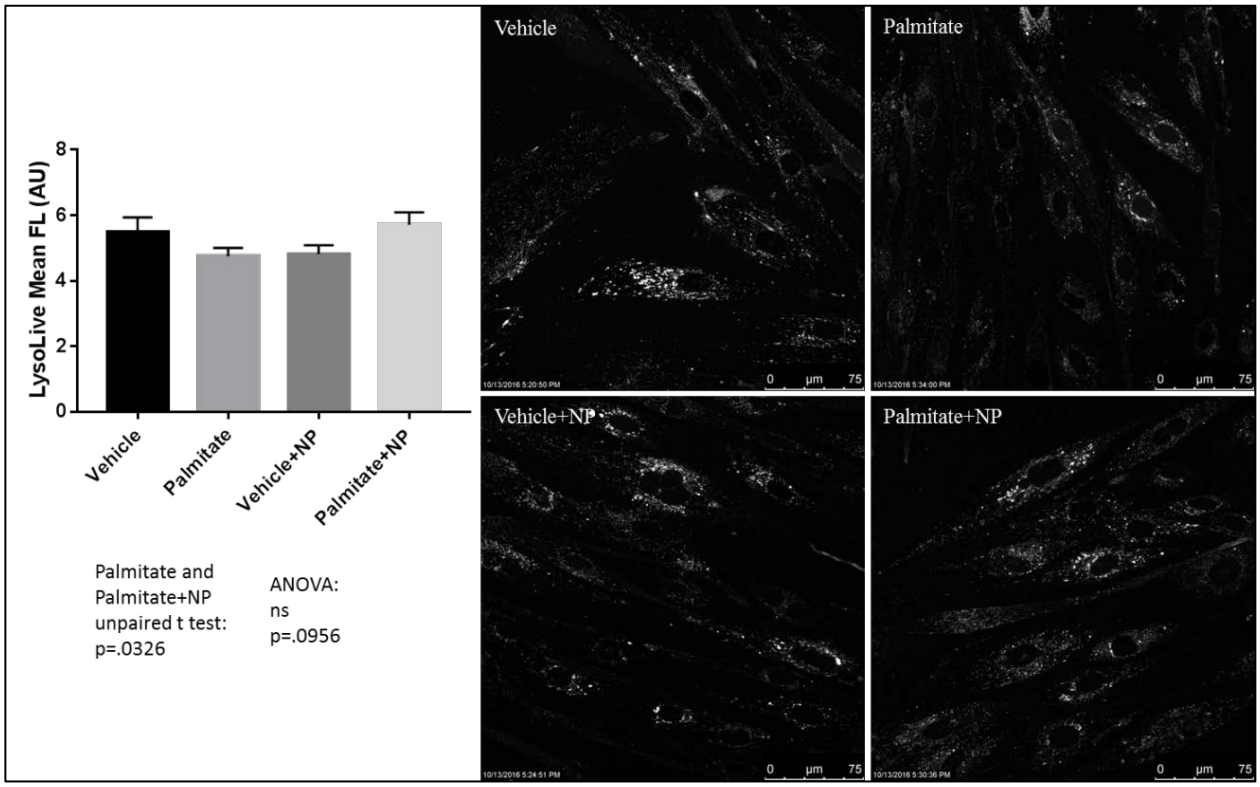

Figure 19: CM lysosomal phosphatase activity measurement after a 4 hour palmitate treatment with a prior **24 hour pre-palmitate treatment of PLGA nanoparticles with surface adsorbed PEI**. Graph of mean cellular fluorescence of LysoLive live cell confocal imaging, with representative images. Viable cells analyzed from two images from one experiment. N's: Vehicle = 32, Palmitate = 50, Vehicle+NP = 43, Palmitate+NP = 36. Cells with internalized nanoparticles (NPs) only analyzed in NP treatment groups. Error bars indicate SEM.

In accordance with pH data, nanoparticles without surface adsorbed PEI were tested for a 24 hour pre-palmitate incubation to determine the effect of increased time for PLGA degradation upon phosphatase activity without the proton-sink effect of PEI, albeit with shorter duration in lysosomes (Figure 4). Qualitative results indicate that nanoparticle treated groups with or without palmitate treatment showed increased phosphatase activity (Figure 20). **Specifically, a 24 hour pre-palmitate nanoparticle treatment without PEI surface adsorption to PLGA produced observable increases in phosphatase activity.** These results indicate that the

trending decrease in lysosomal pH for PLGA nanoparticles without PEI (Figure 16) **did produce** an observable increase in lysosomal degradative function (Figure 20).

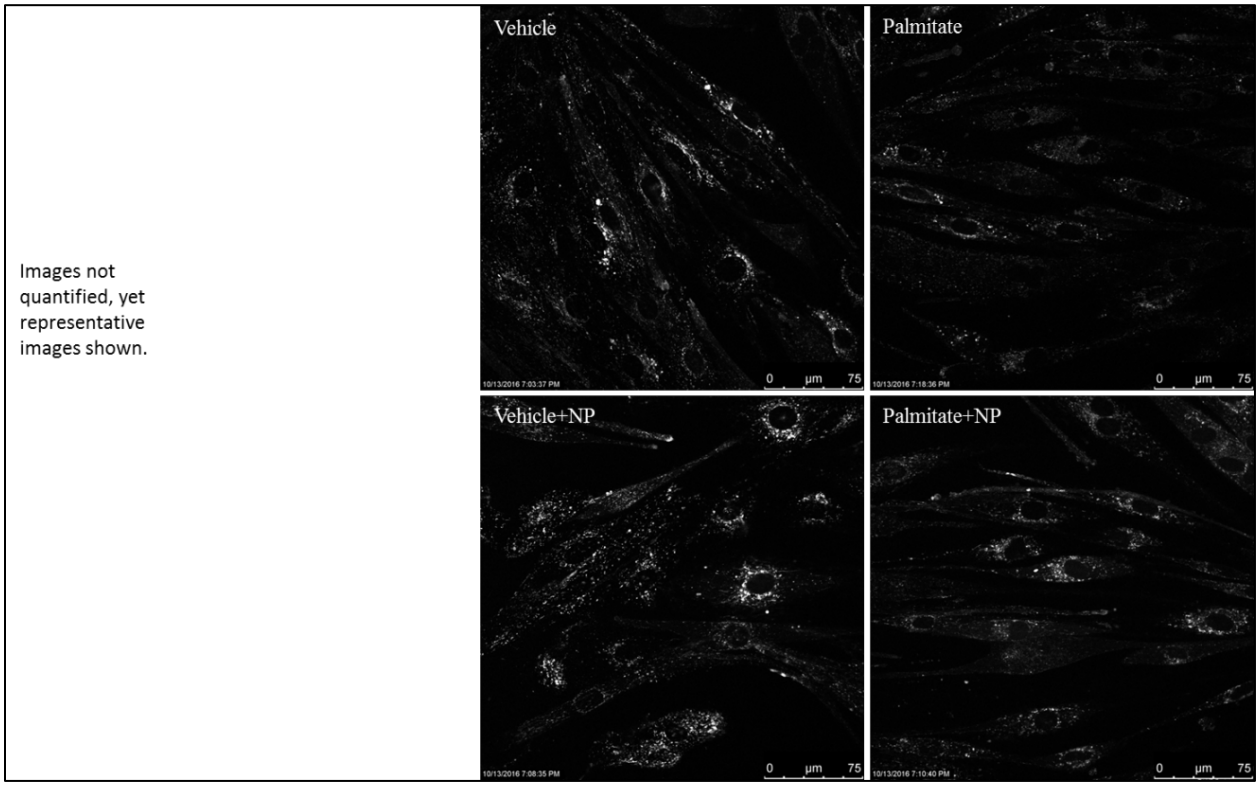

Figure 20: CM lysosomal phosphatase activity measurement after a 4 hour palmitate treatment with a prior **24 hour pre-palmitate treatment of PLGA nanoparticles without surface adsorbed PEI**. Graph of mean cellular fluorescence of LysoLive live cell confocal imaging, with representative images. Viable cells analyzed from two images from one experiment. N's: Vehicle = , Palmitate = , Vehicle+NP = , Palmitate+NP = . Cells with internalized nanoparticles (NPs) only analyzed in NP treatment groups. Error bars indicate SEM.

In summary, PLGA nanoparticles with or without PEI produced observable and quantitative increases in lysosomal enzyme activity at short and long incubations to differing degrees possibly related to PEI influenced nanoparticle uptake, distribution and proton absorption. Consistent trends of increased enzyme activity in the presence of palmitate with prior nanoparticle treatment **substantiate the claim that nanoparticle can modulate lysosomal pH** in an extent to which enzyme activity is influenced.

Importantly, autophagic flux is dependent on the degradation of autophagosomes and their cargo. So, increases in lysosomal enzyme activity will theoretically increase or restore

autophagic flux to basal levels. Here, treatment with PLGA nanoparticles demonstrated that lysosomal enzyme activity can be modulated upon CM PLGA nanoparticle uptake.

Explanations for variance seen in lysosomal pH change and enzyme activity dependent on pre-palmitate nanoparticle treatment time and nanoparticle surface coating: Due to the evidence that cathepsin L and phosphatase activity is increased at 8 hours of nanoparticle pre-palmitate treatment yet non-significant but trending restoration of pH is observed for this treatment, LysoSensor Green probes may not be sensitive enough to measure the change in pH that is giving rise to increased cathepsin L and phosphatase activity. Additionally, the acid released from the nanoparticles may be influencing these enzymes in the immediate environment of the nanoparticle, creating a microenvironment of reduced pH where there is then an observed increased activity in cathepsin L and phosphatase. Further, after 24 hours of nanoparticle pre-palmitate treatment with the same PEI surface adsorption, a more robust and significant reduction in pH is observed as measured by LysoSensor Green. Thus, the longer and theoretically more rapid release of acidic monomers from the PLGA nanoparticles may then be decreasing the pH to a level where the LysoSensor Green probe can then detect the change in pH. **This sustained and rapid release of acid before palmitate is presented to the cells in a lipid-overload concentration may be required to have measureable, by current methods, change in pH.**

The degradation rate of PLGA nanoparticles may be increased at later treatment time points due to increased internal acid catalyzed hydrolysis, lower relative molecular weight, and pore formation for increased hydrolysis in the nanoparticle relative to that of earlier time points [52]. This increased degradation rate and subsequent increased release of acidic monomers may be enough to produce a measureable change in pH, even when proton flux across lysosomal

membranes is rapid. It has been shown that acidification can occur on the order of seconds in neuronal synaptic vesicles when the endogenous vATPase is inhibited by bafilomycin [66]. This was determined using optically activated proton pumps. In light of this time scale for acidification with impaired vATPases, albeit cell-type-specific, **rapid and sustained** degradation of PLGA nanoparticles may produce the needed change in pH for increased enzyme activity.

With this in mind, **proton saturation** of nanoparticle surface adsorbed PEI due to PEI's "proton-sink" characteristics may allow nanoparticle release of protons to **effectively** reacidify the lysosome, since the proton-sink of PEI has been exhausted. This proton saturation of PEI may occur after 8 hours of pre-palmitate nanoparticle treatment, and thus may be an additional factor in the sensitivity of lysosomal pH measurement. Meaning, once the PEI is saturated, a measureable change in pH can be determined, with current data suggesting a 24 hour pre-palmitate nanoparticle treatment is adequate to produce a measurable change in pH.

An additional explanation of this nanoparticle treatment time dependence is increased nanoparticle lysosomal escape and recovery after 24 hours of nanoparticle pre-palmitate treatment. Early nanoparticle escape from the endo-lysosome pathway within the first 8 hours may be recovered by sequestration of the nanoparticles and relocalization to the lysosomes for acid release measured for 24 hour pre-palmitate nanoparticle treatments. PEI may be a mediator in this pathway since early escape of the nanoparticle from the lysosome may be mediated by the proton-sink effect of PEI [67]. Upon nanoparticle escape from the lysosome, the PEI on the nanoparticle may be saturated with protons from the cytosol. Subsequent sequestration of the cytosolic nanoparticle and trafficking to the lysosome may produce a nanoparticle adequately prepared for functional acid release since the saturated PEI is no longer absorbing protons released from the nanoparticle.

The idea that LysoSensor Green is less sensitive at 8 hours of nanoparticle pre-palmitate treatment is due to the inability of LysoSensor Green to detect smaller changes in pH when extra influences, such as time for degradation, degradation rate, uptake and PEI are present. Meaning, the pKa of LysoSensor Green and its corresponding sensitivity standard curve are very important in determining the change in pH at particular nanoparticle treatment times (one cannot have micrometer sensitivity when using a meter scale). The dynamic range of the probe can be explored by using pH clamped lysosomes, yet even the ionophores used for these measurements may perturb lysosome biology so the sensitivity displayed may not be the same as that of nanoparticle treatment with or without the presence of palmitate [68].

Biological data dependent on pH, such as enzyme activity, supports the effect of PLGA nanoparticles on lysosomal luminal pH even though the LysoSensor Green probe may be less sensitive to pH change for an 8 hour pre-palmitate nanoparticle with PEI treatment. Even if LysoSensor Green data continues to be variable, a summation of data from enzyme activity and autophagic flux supports/determines PLGA nanoparticle's ability to influence lysosomal pH.

V.6 Restoration of Autophagic Flux by PLGA Nanoparticles

Due to results indicating significant decreases in lysosomal pH and increases in lysosomal enzyme activity upon nanoparticle treatment when CMs are treated with palmitate, autophagic flux assessment was performed on the same sets of nanoparticles and treatment times to determine the additive effect of these data on autophagosome turnover. Specifically, double fluorophore tagged microtubule-associated protein 1 light chain 3 beta (mCherry-GFP-LC3) autophagosome marker protein confocal microscopy in live CMs was performed. mCherry-GFP-LC3 fluorescence is dependent on the pH of its microenvironment. Specifically, when the

autophagosome bound LC3 protein is not fused with the lysosome both fluorophores mCherry and GFP fluoresce. However, upon autophagosome fusion with the lysosome, GFP fluorescence is quenched but not mCherry. These markers for autophagosome-to-lysosome passage give a proper view of autophagosome flux as well as an indirect measurement of lysosomal pH [62]. Quantification of these events by puncta colocalization analysis is described in Section VI.4. Decreased CM number with GFP puncta colocalized to mCherry puncta per image indicate restored autophagic flux.

For an 8 hour pre-palmitate nanoparticle treatment with PEI surface adsorption, autophagic flux was significantly restored in the presence of palmitate challenge (Figure 21). These results indicate that the quenching of GFP was restored by the reacidification of lysosomes by PLGA nanoparticles. Subsequent increased degradation of LC3 labeled autophagosomes by lysosomes indicates restored autophagic flux by PLGA nanoparticle treatment. Interestingly, 8 hour pre-palmitate nanoparticle with PEI treatment did not fully restore autophagic flux, however a significant decrease in CMs with GFP puncta colocalized to mCherry puncta is observed per image taken. These results indicate that PLGA nanoparticles with surface adsorbed PEI in an 8-hour pre-palmitate treatment regimen partially restore autophagic flux by mechanisms of decreased lysosomal pH and increased lysosomal enzyme activity in the presence of palmitate.

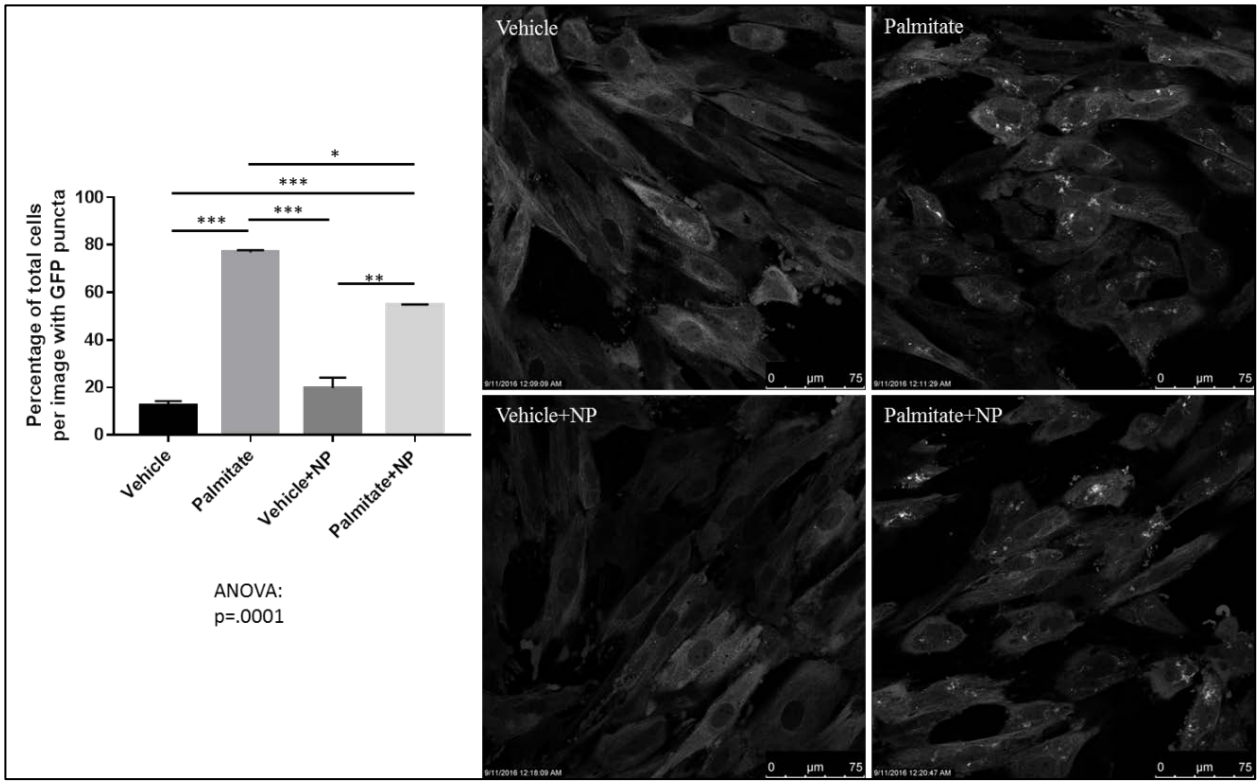

Figure 21: CM autophagic flux assessment after a 4 hour palmitate treatment with a prior **8 hour pre-palmitate treatment of PLGA nanoparticles with surface adsorbed PEI**. Confocal fluorescent imaging of mCherry-GFP-LC3 retroviral expression in live CMs. GFP puncta quantification and representative images. Graph represents percentage of total cells per image that have colocalized GFP puncta with that of mCherry. Cells with internalized nanoparticles only analyzed in NP treatment groups. Two images per group were analyzed from one experiment. Error bars indicate SEM.

Longer incubation periods were also measured for PLGA nanoparticles with and without PEI surface adsorption to fully understand the effect of increased PLGA degradation on autophagic flux in comparison to lysosomal pH and enzyme activity data.

A 24 hour pre-palmitate treatment of nanoparticles with PEI surface adsorption produced similar results as that of an 8 hour pre-palmitate treatment (Figure 22). These results agree with previous data of significantly decreased pH and increased enzyme activity in CM lysosomes for this particular nanoparticle treatment regimen. In comparison to the 8 hour pre-palmitate treatment, longer incubation with nanoparticles produced a larger decrease in CMs with GFP puncta colocalized with mCherry puncta per image, as depicted by the non-significant difference

between Vehicle and Palmitate+NP groups in Figure 22. These results correlate well with the observed higher pH change in CM lysosomes treated for 24 hours prior to palmitate challenge compared to that of an 8 hour pre-treatment. **Consequently, an increased nanoparticle incubation period of 24 hours produces a more substantial restoration effect on autophagic flux when treating CMs with PEI coated PLGA nanoparticles.**

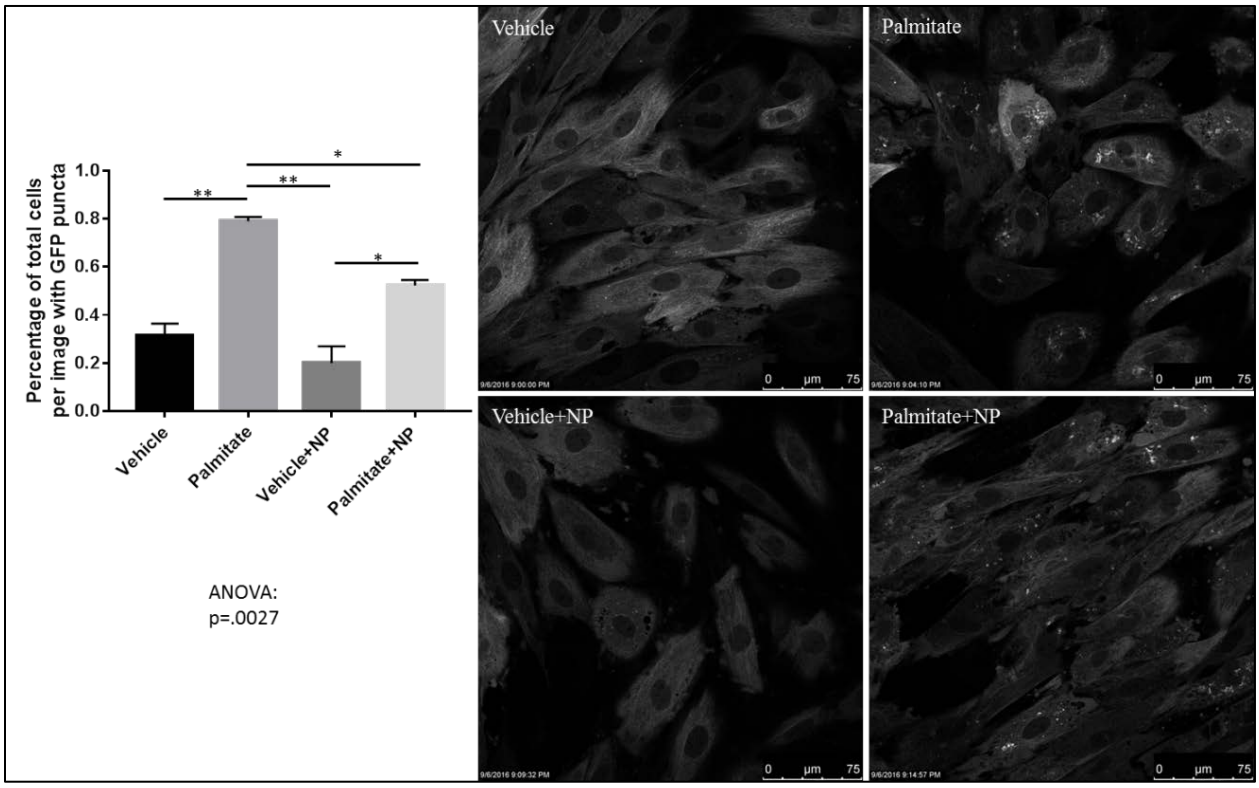

Figure 22: CM autophagic flux assessment after a 4 hour palmitate treatment with a prior **24 hour pre-palmitate treatment of PLGA nanoparticles with surface adsorbed PEI**. Confocal fluorescent imaging of mCherry-GFP-LC3 retroviral expression in live CMs. GFP puncta quantification and representative images. Graph represents percentage of total cells per image that have colocalized GFP puncta with that of mCherry. Cells with internalized nanoparticles only analyzed in NP treatment groups. Two images per group were analyzed from one experiment. Error bars indicate SEM.

A 24 hour incubation with nanoparticles **without PEI** surface adsorption **did not produce** a significant increase in autophagic flux compared to palmitate alone (Figure 23). This is in agreement with lower acidification observed in lysosomal pH measurement for this treatment, but does not correlate with observed increased phosphatase activity when CMs are treated with

nanoparticles without PEI for 24 hours prior to palmitate treatment. **However, as lysosomal pH determines lysosomal enzyme activity and a trending yet non-significant decrease in pH was measured when CMs were treated with this set of nanoparticles, the increased enzyme activity may be an indication of the early stages reacidification and autophagic flux restoration.** Importantly, when looking at the individual data points in Figure 23, an outlier increases the mean Palmitate+NP number of CMs with GFP puncta colocalized with mCherry puncta percentage per image, indicating that autophagic flux may be restored upon further analysis of longer treatment periods.

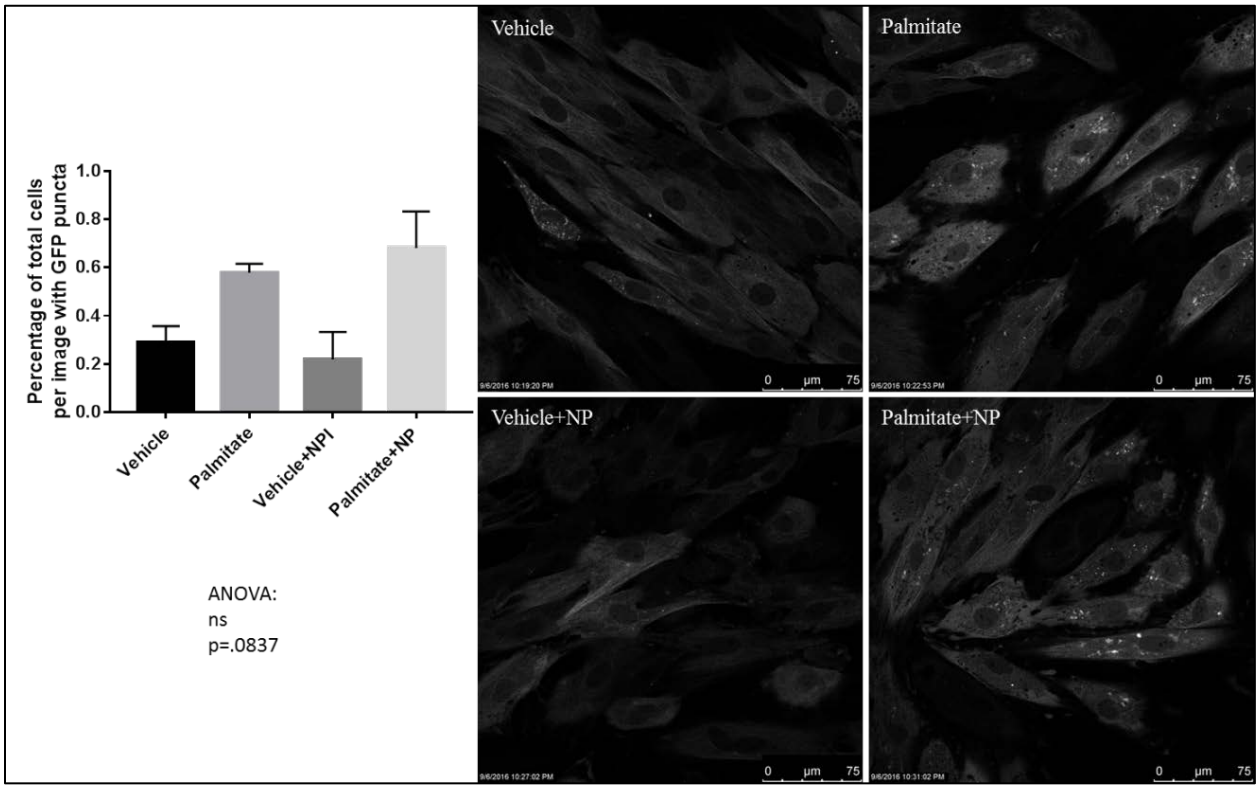

Figure 23: CM autophagic flux assessment after a 4 hour palmitate treatment with a prior **24 hour pre-palmitate treatment of PLGA nanoparticles without surface adsorbed PEI**. Confocal fluorescent imaging of mCherry-GFP-LC3 retroviral expression in live CMs. GFP puncta quantification and representative images. Graph represents percentage of total cells per image that have colocalized GFP puncta with that of mCherry. Cells with internalized nanoparticles only analyzed in NP treatment groups. Two images per group were analyzed from one experiment. Error bars indicate SEM.

V.7 Autophagosome Marker Protein Analysis upon PLGA Nanoparticle Treatment

As previously described in Section V.2, autophagosome marker protein levels are used to better understand autophagic flux. This analysis was performed for the three nanoparticle treatment regimens described in this thesis. In Figure 24, little to no change in autophagosome marker proteins upon each nanoparticle treatment is observed. However, there is a slight decrease in p62 of palmitate treated CMs with a 24 hour pre-palmitate treatment of PLGA nanoparticles **without** surface adsorbed PEI compared to its vehicle control. Additionally, a small decrease in LC3-II is seen in vehicle treated CMs with this nanoparticle group compared to vehicle without nanoparticle treatment. A similar decrease is seen with a 24h pre-palmitate nanoparticle with PEI treatment vehicle comparison. This is correlates with additional data from mCherry-GFP-LC3 fluorescence, where nanoparticle-containing CMs with or without palmitate treatment had slightly lower levels of mCherry, albeit not consistent with all CMs containing nanoparticles (Figure 25).

Additionally, p62 levels have an observable increase in experimental groups treated with any of the nanoparticle treatment regimens. This suggests a possible mechanism of autophagic labeling of the nanoparticles themselves by p62. It is possible that cytosolic nanoparticles can be labeled by p62 for trafficking to the autophagosome for degradation, since PLGA itself or the PEI surface coating may be ubiquitinated.

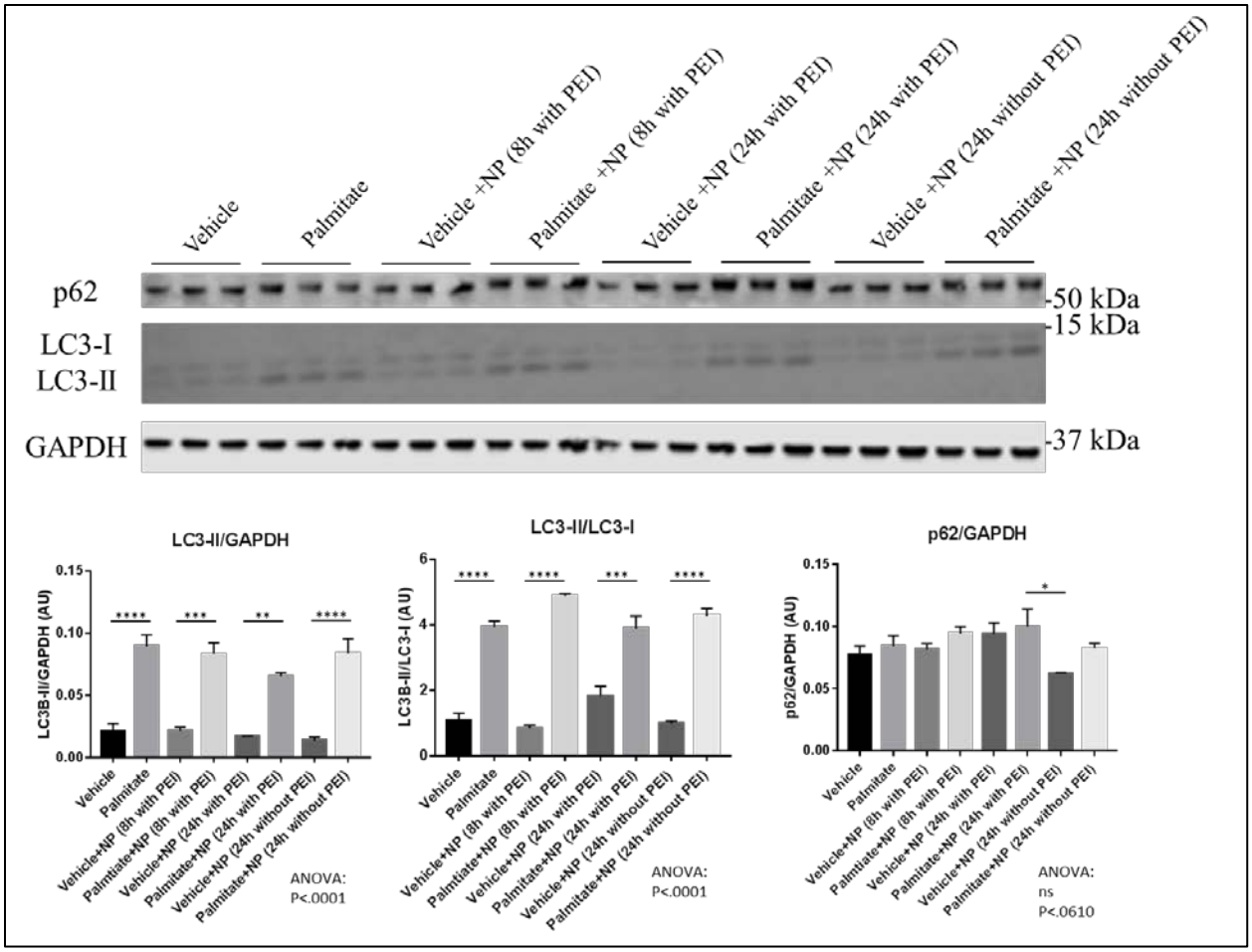

Figure 24: Autophagosome marker protein levels of CMs treated with the three nanoparticle treatment regimens described in this thesis. Specifically, 8 hour pre-palmitate treatment of PLGA nanoparticles (NPs) with surface adsorbed PEI (**8h with PEI**), 24 hour pre-palmitate treatment of PLGA nanoparticles with surface adsorbed PEI (**24h with PEI**), and 24 hour pre-palmitate treatment of PLGA nanoparticles without surface adsorbed PEI (**24h without PEI**). Relative differences in protein levels for this **one** blot were statistically determined (error bars SEM). For brevity, significance is only indicated between vehicle and palmitate for each NP or control group for LC3-II/GAPDH and LC3-II/LC3-I. Additionally for LC3-II/GAPDH and LC3-II/LC3-I, all vehicle and palmitate groups were significantly different between NP or control groups. For p62/GAPDH, the only significance indicated by multiple comparisons after ANOVA is shown.

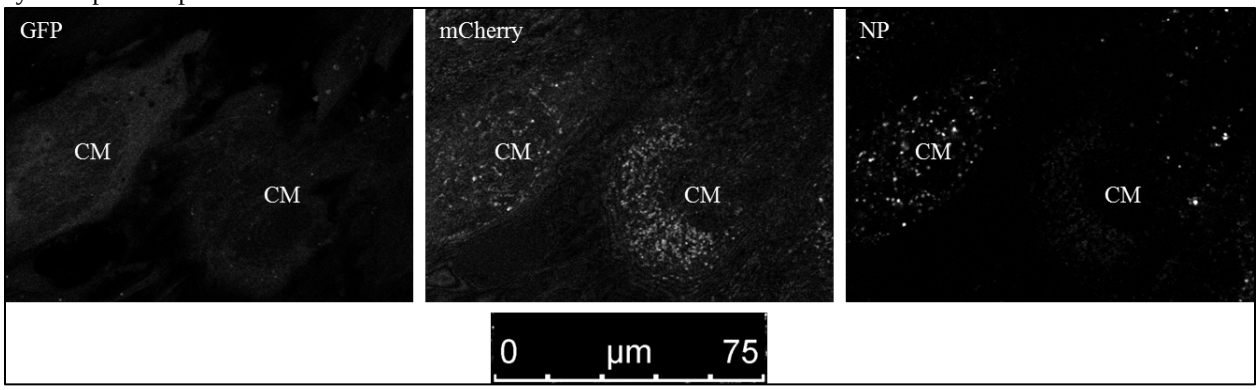

Figure 25: Select CMs were internalized nanoparticles (NPs) decrease mCherry puncta. Live CM confocal imaging of mCherry-GFP-LC3 retroviral levels in vehicle with a prior 24 hour pre-vehicle nanoparticle without surface adsorbed PEI treatment.

Nanoparticle treatment did not affect autophagy machinery as demonstrated by unchanged levels of phosphorylated and total mTOR and Beclin-1, albeit not tested for any of the nanoparticle treatment regimens in this thesis (data from a nanoparticle design iteration not shown).

V.8 Summary, Future Directions and Limitations

PLGA nanoparticles can be engineered to produce a reacidification effect in CM lysosomes to subsequently restore enzyme activity and autophagic flux in the presence of palmitate induced lipotoxicity. By reducing PLGA's molecular weight for increased degradation rate, targeting clathrin mediated endocytosis, including free glycolic acid for increased degradation, and reducing nanoparticle uptake duration with PEI surface adsorption, nanoparticles were able to restore lysosomal function at various nanoparticle treatment lengths in the context of lipotoxicity in CMs.

A 24 hour pre-palmitate PLGA nanoparticle treatment with surface adsorbed PEI demonstrated the most consistent results in restoring autophagic flux across the assays presented in this thesis. This could be due to longer residence and subsequent more acid release within lysosomes, dictated by PEI mediated nanoparticle uptake. PLGA degradation rate may also be increased upon longer residence within the lysosome compared to that of nanoparticles without PEI for the same pre-palmitate treatment period, due to higher potential of acid-catalyzed hydrolysis. Shorter incubation periods of nanoparticles with PEI surface adsorption also demonstrated increased lysosomal enzyme activity and restored autophagic flux. Nanoparticles without PEI surface adsorption did not perform as robustly in terms of restored autophagic flux, but did demonstrate enzymatic restoration and a partial lysosomal pH decrease.

In this thesis, CMs were engineered with biomaterials as a proof-of-principle approach to restore autophagic flux in an acute lipotoxic cardiomyopathy model. This PLGA nanoparticle therapy can be further designed to utilize natural cellular uptake mechanisms, such as the adsorption of transferrin to the nanoparticle surface to target transferrin receptors on CMs. This will **remove** the proton-sink effects of PEI and provide a clear understanding of PLGA nanoparticle degradation in lysosomes. Nanoparticles can also be incorporated with pH sensors, whereby error-prone commercially available pH probes can be avoided. Here, detection of PLGA degradation to the surrounding lysosomal lumen can be quickly determined to better design PLGA for rapid degradation.

Nanoparticle delivery to CMs can also be targeted *in vivo* by a newly identified CM specific peptide [69]. This peptide can be covalently conjugated to the surface of the PLGA nanoparticles and subsequently act as a targeting mechanism to CM membrane receptors, or as a cell penetrating peptide. This design will readily provide translational potential of the FDA approved PLGA nanoparticles by allowing targeted delivery to CMs from an intravenous administration for modulation of lipotoxicity in patients presenting obesity and early stages of cardiomyopathy.

This thesis did not directly quantify the number of nanoparticles colocalized with lysosomes. Therefore, the stoichiometric proportion of nanoparticles within lysosomes for optimal acidification was not determined. Additional ways to address whether or not nanoparticles did indeed colocalize with lysosomes can be done by a virtual SEM or real SEM, were a slice from a z-stack can be analyzed for fluorophore overlap, or upon direct nanoparticle analysis, respectively. These are additional ways to ensure that the nanoparticle is **within** the lysosome. Cytosolic nanoparticle trafficking events were not analyzed, so it is possible that a cytosolic nanoparticle could be trafficked to the lysosome due to charge differences.

Nanoparticle design optimization techniques were based on theoretical conclusions that would increase acid release. These were rapidly iterated to develop a PLGA nanoparticle with the greatest acidification potential. Since there was not a validated and trustworthy pH measurement system in place while iterating through the nanoparticle design due to prolonged quantitative method optimization, there was not a comprehensive side-by-side comparison for each theoretical conclusion that increased degradation rate (acid release), such as the addition of free glycolic acid. The supplier, however, suggested this to increase PLGA degradation rate.

Acidification potential of PLGA nanoparticles with theoretical optimized degradation rate was determined within lysosomes, since this is where the physiologic effect of increased acid release is desired. Some acidification potential experiments were conducted outside cells, yet these assays were not sensitive enough to produce a reliable signal. Since small amounts of released acid from PLGA nanoparticles can possibly influence its immediate microenvironment, such as the enzymes immediately adjacent to the nanoparticle, these extracellular assays could most likely not detect this small pH change. Thus, the acidification potential was thought to be most relevant if determined within CM lysosomes.

Repeat experiments **must be conducted** to ensure the repeatability of these data. Meaning, the data from pH, enzyme and autophagic flux fluorescent experiments were from one experiment from each assay (as listed in all figure legends), with some repeats not included but guiding selection of the representative experiment to present in this thesis. Due to shortage of time when writing this thesis due to an incredible amount of nanoparticle optimization and equipment limitations, additional experiments have not been analyzed and included, but a brief observation of repeat experiments suggests that the 24 hour pre-palmitate PLGA nanoparticle with PEI surface adsorption treatment regimen does indeed restore autophagic flux.

Section VI Methods

VI.1 Lysosomal pH Measurement

Multiple experimental approaches to measure lysosomal pH in differentiated H9c2 cardiomyoblasts (CMs) at the University of Iowa were performed to determine a reliable and quantitative florescence based method. Table 3 lists attempted fluorescence based approaches and reasons for iterative exploration of a robust and reliable method.

In this analysis for a reliable method to measure live CM lysosomal pH with the current confocal microscopy, LysoSensor Green produced the most reliable pH change measurement albeit less quantitative than other ratiometric approaches. To create a more quantitative pH measurement, LysoTracker Blue was measured in parallel to LysoSensor Green as described in Section VI.4. Normalized images to LysoTracker Blue can better quantitate lysosomal pH by normalizing for lysosome size and number, if these two remain the same between groups [65]. However, the pH independent uptake of LysoTracker Blue was modulated by chloroquine treatments, indicating possible disruption of the probe itself or disruption in the probe uptake mechanism due to possible perturbed lysosomal biology from chloroquine treatment. Additionally, lysosomal size varied between vehicle and palmitate groups, as discussed in Section V.4. Thus, LysoTracker Blue data is an important metric when determining lysosomal biology, number and size, but is not adequate to normalize LysoSensor Green fluorescence.

In summary, LysoSensor Green florescence produced a semi-quantitative measurement of lysosomal pH, with an adequately dynamic range of pH measurement shown by the control groups of palmitate, vehicle and co-treatment with chloroquine. However, small changes in pH were difficult to delineate upon nanoparticle treatment due to limitations in the sensitivity of this probe to detect **small** changes in pH. However, taken together with LysoTracker Blue data, albeit

not normalized to LysoTracker Blue data, LysoSensor Green fluorescence did produce the most reliable method to measure pH in CM lysosomes with currently available equipment at the University of Iowa.

Table 3: Measurement methods of pH used to determine the best available technique for measurement of lysosomal pH at the University of Iowa under live cell experimental conditions. (CQ = chloroquine, NP = nanoparticle)

Platform of Measurement	Fluorescent Probes Used	Optimization Techniques Attempted	Outcome
Fluorescence Plate Reading (SpectraMax) **Live cells**	LysoSensor Yellow/Blue non-dextran ratiometric probe (pH dependent emission if excited at 355nm, the isosbestic point)	1. Increased concentrations to overcome background fluorescence in the blue channel. 2. Consistent measurement settings. 3. Black-walled, clear bottom 96 well plates with monolayer of differentiated (5 days) H9c2 cardiomyoblasts (CMs). 4. Use of high and low pH calibration buffers with ionophores to clamp lysosomal pH. 5. Multipoint scan with 6flashes/read produced more consistent measurements over that of an endpoint scan with 100flashes/read.	Dynamic range of pH measurement slightly exhibited when using pH calibration buffers, yet experimental groups out of this range indicating high noise produced by very low signal to noise for this specific plate reader, despite reported success of this method in the literature [7]. Thus, this method **was not used** for analysis of pH.
Fluorescence Plate Reading (SpectraMax) **Live cells**	LysoSensor Green (pH dependent) LysoTracker Blue (pH independent) Used both individually and for ratiometric analysis	Same as for LysoSensor Yellow/Blue.	Experimental groups slightly within dynamic range of measurement when using pH calibration buffers (pH 3.25 and 6.36) for the LysoSensor Green probe. However, vehicle signal was very close to pH 6.36, indicating CM lysosomes treated with vehicle have a high pH, or the calibration buffer effects the LysoSensor Green probe's ability to fluoresce, which **is not** reported in the literature. LysoSensor Green did not respond to CQ treatment as expected, possibly **due to increased lysosome size**, but this was disproved by **reduced LysoTracker Blue signal**. Possible explanation could be the inability of CQ treated lysosomes to take up LysoTracker Blue. Caution used when interpreting data from this assay, but experimental groups have lower noise than LysoSensor Yellow/Blue. Ratiometric comparison of LysoSensor **Green/LysoTracker Blue indicated some recovery with NP, but LysoSensor Green signal alone indicates the opposite.** Additionally, the ratio for CQ treated CMs is high, pointing to the sensitivity of this assay as possible **artifact.** Thus, this method **was not used** for analysis of pH.
Confocal Microscopy Multiphoton Leica SP5 **Fixed Cells**	LysoSensor Yellow/Blue dextran ratiometric probe (pH dependent emission if excited at 355nm, the isosbestic point)	Varied multiphoton excitation wavelength.	Multiphoton excitation can achieve the isosbestic excitation of this probe, yet upon further inquiry, the fixing of the cells due to the upright nature of the scope inactivated the **live lysosomal pH sensing ability of the probe**. In other words, the emission seen would just exhibit the pH of the fixing buffer. Thus, this method **was not used** for analysis of pH.

Table 3: Continued

Confocal Microscopy Leica SP8 **Live cells**	LysoSensor Yellow/Blue dextran ratiometric probe (pH dependent emission if excited at 355nm, the isosbestic point)	Multiple optimization experiments under the guidance of CMRF staff who suggested that a 405nm excitation of the probe is adequate.	Not used for analysis due to the **non-isosbestic excitation** of the probe. A 405nm excitation is **not adequate** for robust or reliable measurement of pH, since at this wavelength, **the excitation is dependent on pH**, thus **skewing the already pH dependent emission**. Thus, this method **was not used** for analysis of pH.
Epifluorescence Olympus IX81 **Live cells**	LysoSensor Yellow/Blue ratiometric probe (pH dependent emission if excited at 355nm, the isosbestic point)	Correct emission filters were available in this microscope, as well as the proper isosbestic excitation wavelength of 355nm.	Microscope sensitivity not adequate for ratiometric analysis. Very high background fluorescence. Thus, this method **was not used** for analysis of pH.
Flow Cytometry ARIA **Live cells**	LysoSensor Yellow/Blue dextran ratiometric probe (pH dependent emission if excited at 355nm, the isosbestic point)	Correct emission filters were available in this flow cytometer, as well as the proper isosbestic excitation wavelength of 355nm. **Increased concentration** of probe to **overcome** background fluorescence.	High background in blue emission wavelength yielded high noise in data with little variability in experimental groups. Additionally, **pH calibration buffer treated cells exhibited little dynamic range with experimental groups well out of range.** Thus, this method **was not used** for analysis of pH.
Confocal Microscopy Leica SP8 **Live cells**	Oregon Green 514 ratiometric probe (pH dependent excitation at 514nm - used as a ratiometric probe normalized to excitation at 458nm)	Optimized concentration and treatment time.	**Sensitivity of probe not adequate for lysosomal pH** measurement, as exhibited by **high variability** between multiple experiments. **Possible explanation:** high background seen in excitation wavelength (458nm). Thus, this method **was not used** for analysis of pH.
Flow Cytometry ARIA **Live Cells**	LysoSensor Green (pH dependent) LysoTracker Blue (pH independent) Used both individually and for ratiometric analysis	Correct emission filters were available in this flow cytometer.	pH calibration exhibited a **measurable response** with this flow cytometer when analyzed ratiometrically. **This result led to the pursuit of confocal imaging with these probes.**
Confocal Microscopy Leica SP8 **Live cells**	LysoSensor Green (pH dependent) LysoTracker Blue (pH independent) Used both individually and for ratiometric analysis.	Optimized concentrations (1uM/probe) and treatment times (1h). Imaged in HEPES based imaging buffer with 10% FBS. Imaged at RT, with total imaging time up to 20 minutes.	Due to the qualitative fluorescent data from LysoSensor Green (dependent on loading concentration), LysoTracker Blue was used a normalizer due to its reported non-pH dependent uptake This method exhibits **some variability** from experiment to experiment, but reliably demonstrates lysosomal pH change in experimental groups, confirmed by CQ treatment measured by LysoSensor Green. However, CQ treatment also highly reduces LysoTracker Blue signal. Since LysoTracker Blue single did vary with CQ treatment, i.e. large increases in pH, as well as disproportionately with lysosomal size, **normalized** LysoSensor Green data to LysoTracker Blue **was not considered** representative of changes in pH. However, LysoTracker Blue data is representative of lysosomal number, biology and size, therefore a valuable readout when looking at LysoSensor Green data. **This method (only LysoSensor Green intensities) was used to measure pH as presented in this thesis.**

VI.2 PLGA Nanoparticle Formulation

Optimized methods for nanoparticle formulation stem from previously described single emulsion solvent extraction/evaporation techniques [55, 70]. Briefly, poly(DL-lactide-co-glycolide) carboxylic acid terminated 4.6kDa statistical (random) block copolymer (PLGA, Lactel Absorbable Polymers B6013-1) was dissolved in the organic solvent dichloromethane (DCM, Sigma 676853) with the addition of free glycolic acid (Sigma 124737) and lipophilic fluorescent probe (DiO and DiD, Molecular Probes V22889). This organic phase was then emulsified in poly(vinyl alcohol) (PVA, Sigma 360627) by ultra-sonication (Branson Sonifier 450 with tip 102C CE). DCM then evaporated under stirring, leaving behind PLGA nanoparticles. Washed nanoparticles were characterized, aliquoted and stored in milliQ at -80C until use, whereupon aliquots were used up to three freeze/thaw cycles. Before use, aliquots were thawed, briefly sonicated in a waterbath sonicator (Fisher Scientific FS20), and vortexed. Polyethylenimine (PEI {branched Mw 25kDa}, Sigma 408727) surface adsorption coatings were performed in a 37C shaking incubator. The step-by-step methodology is listed below.

1. 80mL solutions of filtered 5% w/v PVA in milliQ were placed in 150mL beakers on a plate stirrer at #3.9 stir setting (check exact RPM). If smaller volumes of PVA are used for smaller nanoparticle batches, smaller beakers can be used, e.g. for 40mL 5% PVA solution (for 20mg PLGA), use 50mL beakers.
2. Dissolve 20mg of PLGA in .4mL DCM in a small glass beaker. Add 20mg of free glycolic acid to this mixture (add .2mL of 100mg/mL free glycolic acid in ethanol). Add 3uL of DiO or DiD lipophilic fluorescent probe to this mixture. This organic phase of the nanoparticle emulsion is then sonicated in the water bath sonicator until clear (~30sec).
3. 3mL of the 5% PVA is added dropwise to the organic phase while vortexing in the small glass beaker.
4. This two phase mixture is then ultra-sonicated for 100sec at power 2.5, by using 10-15sec bursts of sonication, with 10sec cool down on ice between.
5. Once sonicated, the emulsified solution is added back to the 5% PVA. A total of 40mg PLGA is added per 80mL 5% PVA, meaning two emulsions are added per 80mL 5% PVA.
6. The 5% PVA is stirred on a stir plate (#3.9 speed) for 6h for adequate DCM evaporation and PLGA nanoparticle hardening. Protect from light.

7. Upon 6h, solutions are spun at 22,000G for 10min. The supernatant is removed, and the pellet is resuspended in 5mL milliQ using water bath sonication and vortexing. This is repeated twice more, for a total of 3 washes to remove the PVA from the nanoparticles.
8. Upon the last resuspension, the nanoparticle pellet is resuspended in 4mL milliQ, aliquoted in .5mL tubes, and frozen at -80C until further use, such as PEI surface adsorption for surface charge modification.
9. For nanoparticle concentration measurement, 100uL of nanoparticle suspension is frozen in a weighed .5mL tube, lyophilized, then weighed. The mass measured by a milligram scale is then used to determine the concentration of the nanoparticle aliquots.
10. For PEI surface adsorption for surface charge modification from negative (carboxylic acid end group) to positive charge, nanoparticle aliquots are thawed and subjected to .0025% PEI incubation at 37C in a 250RPM shaker for 4h.
11. Modified nanoparticles are then spun down and washed twice (1mL milliQ at 22,000G for 6min, waterbath sonicate 5sec then vortex to further break up pellet, then waterbath sonicate for 10sec for best resuspension of pellet). For the final resuspension (1mL milliQ) after the last wash, nanoparticles in 1mL milliQ were spun at 1G to remove large particles and aggregates. Subsequent supernatant was the aliquoted as before, with inclusion of 100uL in weighed tube to quantify nanoparticle concentration. Unmodified nanoparticles were incubated and spun at 1G (no addition of milliQ or washing) in parallel with the modified nanoparticles to ensure comparability.
12. Nanoparticle size and surface charge (zeta-potential) were measured using a Zetasizer Nano ZS (Malvern). 40uL of nanoparticle suspension from a frozen aliquot was suspended in milliQ to a final volume of 1mL. Size measurements were taken (2 per sample), then the zeta-potential was measured from the same measurement solution using a folded capillary cell (Malvern DTS1070).
13. Nanoparticle aliquots were thawed, waterbath sonicated for 5sec and vortexed before use in cell culture applications. Three freeze/thaw cycles was considered maximum for lowest nanoparticle aggregation when reusing aliquots.

VI.3 Cell Culture

Cell culture techniques were developed for optimized collection of fluorescent and Western Blot data. H9c2 cardiomyoblast (ATTC CRL-1446) culture methods were developed from [3]. Briefly, cardiomyoblasts from passage 17-22 were plated on 6 well plates treated for cell adhesion (CELLSTAR 657165) or 4 well chambered coverglass slides treated with collagen type 1 (#1.5, LABTEK II 155382) for cell harvest and fluorescence microscopy respectively. Cells were counted and plated in high glucose Dulbecco's Modified Eagle's Medium (HG

DMEM, Gibco 11965-092) supplemented with 10% v/v fetal bovine serum (FBS, Atlanta Biologicals S11150) at 20,000 cells per well in the 4 well slides, and from 15,000 to 45,000 cells per well in the 6 well plates. Upon observance of 75-80% confluency in 4 well sides or 55%-60% confluence in 6 well plates, the plating media was removed. Cardiomyoblasts were washed 3 times in differentiation media, specifically low glucose Dulbecco's Modified Eagle's Medium (LG DMEM, Gibco 11885-084) supplemented with 1% v/v FBS and 10nM all-trans retinoic acid (Sigma R2625). Differences in confluency at the start of differentiation were chosen to enable higher numbers of cells to be imaged than needed for cell harvest. Differentiation of the cardiomyoblasts into cardiomyocytes (CMs) was performed for 5 days, with media changes on the second and fourth days.

Near 4.5 days of differentiation, nanoparticle and palmitate treatments were performed, to have a total ~5 days of differentiation upon fluorescent microscopy or cell harvest. Specifically, nanoparticles (NPs) were added directly to differentiation media at a dose of (.0625)*CD (CD = .0053333mg NP/cm^2 growth area) for PEI surface adsorbed nanoparticles or .428*CD for nanoparticles without surface adsorbed PEI. These doses were determined by fluorescent microscopy to produce adequate nanoparticle uptake and cellular distribution at 8 hour and 24 hour pre-palmitate treatment for PEI treated nanoparticles and at 24 hour pre-palmitate treatment for nanoparticles without PEI treatment. **Adequate nanoparticle uptake and cellular distribution is defined as an equivalent cellular uptake between the two types of nanoparticles at 8 hour pre-palmitate treatment of NPs with PEI compared to 24 hour pre-palmitate treatment of NPs without PEI (see Figure 5), as well as observations that internalized nanoparticles did not outnumber lysosomes (measured by LysoTracker Blue) in untreated cells.**

Palmitate treatments were added after 8 hour and 24 hour treatments with nanoparticles. Specifically, LG DMEM supplemented with 10% v/v FBS and 500uM palmitate (C16:0 hexadecanoic acid Nu-Chek N16A) conjugated to fatty acid free bovine serum albumin (FAF-BSA, Fisher BioReagents BP9704) (1% w/v final FAF-BSA concentration).

Palmitate saturated fatty acid preparations consisted of dissolving palmitate in .1M sodium hydroxide (NaOH, Sigma S5881) for a palmitate concentration of 100mM at 70C. Upon clear suspension, this palmitate-NaOH solution was added to 20% w/v FAF-BSA warmed at 50C for a final palmitate concentration of 10mM. Upon 10 minutes of palmitate conjugation to FAF-BSA at 50C, this palmitate BSA complex was added 1:20 to LG DMEM warmed at 37C and supplemented with 10% v/v FBS for a final working palmitate concentration of 500uM. At the end of nanoparticle treatments when nanoparticles are **adequately internalized**, CMs were washed in this palmitate treatment media 3 times for fluorescence experiments, and 3 times in LG DMEM for cell harvest experiments due to the larger volume of palmitate treatment media needed when washing larger wells. CMs were treated in freshly prepared (right before treatment) 500uM palmitate for **4 hours**, after which fluorescence imaging or cell harvest was performed [3].

Vehicle control conditions consisted of each reagent for palmitate preparation, except that of palmitate. Specifically, vehicle treatment media contained 1% w/v FAF-BSA with .5mM NaOH palmitate solvent in LG DMEM supplemented with 10% FBS.

The control to increase lysosomal pH consisted of the addition of chloroquine directly to vehicle or palmitate treatment after 3 hours of palmitate/vehicle treatment for the final hour. Thus, lysosomal pH was increased by a 1 hour treatment of freshly prepared 80uM chloroquine (chloroquine diphosphate salt Sigma C6628) dissolved in milliQ.

VI.4 Confocal Microscopy

Live cell imaging of the monolayers of differentiated H9c2 cardiomyoblasts (CMs) was performed on an inverted Leica SP8 super resolution confocal microscope in the Central Research Microscopy Facility at the University of Iowa. CMs were washed from palmitate or vehicle treatment containing the probes listed in Table 4 for the particular experiment, placed in 25mM HEPES based imaging buffer, and imaged at 40x after immediate transit to the microscope from the lab (~3 minutes) for a maximum of 20 minutes. On average, a 15 minute imaging period was adequate to obtain 2-3 images per group. Although not temperature controlled, the rapid imaging technique allowed reproducible results from control experiments for the various probes. The pH of the imaging buffer remained constant due to the addition of HEPES, and subsequently reduced CM detachment.

Excitation and emission optimization for each fluorescent channel listed in Table 4 produced well-separated collection of florescence. Channels were tested separately to ensure emission separation for closely emitting probes. For example, the emission of Magic Red for Cathepsin L activity was separated from that of DiO labeled nanoparticles by first testing the probe in cells treated separately with the probe and nanoparticles. Channels for each excitation/emission were collected for each test, to ensure proper channel separation upon the addition of both nanoparticles and Magic Red to one group of cells for measurement of Cathepsin L activity in the presence of degrading PLGA nanoparticles.

Table 4: Excitation and emission settings for the fluorescent probes/proteins used in the data presented in this thesis measured by confocal microscopy.

Fluorescent Probe/Protein	Excitation (nm)	Emission (nm)
LysoLive Phosphatase	490	515-575
Magic Red Cathepsin L	592	628-750
LysoTracker Blue	405	415-450
LysoSensor Green	470	515-545
DiD nanoparticle label	633	643-740
DiO nanoparticle label	488	500-569
mCherry retroviral protein	570	580-620
GFP retroviral protein	488	500-550

LysoLive Phosphatase activity measurement was performed as per the manufacturer's protocol (MarkerGene M1376). Specifically, CM's were treated with .2mM LysoLive reagent added directly to palmitate/vehicle treatment media at the start of the 4 hour palmitate/vehicle treatment. LysoTracker Blue probe was also added directly to the treatment media at 1uM for the final hour to determine lysosomal location.

Magic Red Cathepsin L activity measurement was performed as per the manufacturer's protocol (ImmunoChemistry Technologies 941). Specifically, CM's were treated with .4x of the supplied Cathepsin L substrate with fluorogenic properties for the final 30 minutes of palmitate/vehicle treatment.

LysoTracker Blue fluorescence was measured as per the manufacturers protocol (Molecular Probes L7525). Specifically, 1uM of probe was added to the palmitate/vehicle treatment media for the final 1 hour of incubation. This probe is reported to be internalized and taken up by lysosomes in a **pH independent** manner, yet highly reduced fluorescence upon chloroquine treatment suggested that lysosomal biology as influenced by chloroquine may perturb the uptake of this probe. LysoTracker Blue can be used to locate lysosomes within the cell and determine the lysosomal size and number. These measurements can aid the interpretation of mean cellular fluorescence analysis. Meaning, if LysoTracker Blue cellular mean intensity is higher for a

particular group of cells, this could indicated larger lysosomes and/or a higher number of lysosomes within the cell.

LysoSensor Green fluorescence was measured as per the manufactures protocol (Molecular Probes L7535). Specifically, 1uM of the probe was added to palmitate/vehicle treatment media for the final 1 hour of palmitate incubation. This probe is reported to be internalized and taken up by lysosomes in a **pH dependent** manner, **with increases in intensity indicating decreased pH**. As the pKa of this probe is ~5.2, the probe allowed significant dynamic range when measuring pH change for controls cells. However, when measuring smaller changes in pH as dependent on nanoparticle degradation, the probe yielded variable results as discussed in Section V.5. However, consistent results were obtained and considered in parallel to LysoTracker Blue fluorescence that was collected at the same time. LysoTracker Blue can be thought of as a normalizer for the more qualitative LysoSensor Green measurement, and thus, when lysosomal size and number are consistent between groups, a more quantitative measurement of lysosomal pH can be determined [65]. However, as discussed in Section V.4, the size and number of lysosomes between experimental groups varied so normalization produced false positive results. However, the LysoTracker data is still relevant to understanding the biology of the lysosome under the various treatment conditions.

Nanoparticle fluorescent labeling was optimized for best florescence upon light exposure when treating CMs. Specifically, an optimized amount of DiD or DiO lipophilic stains was added to the nanoparticle formulation as described in Section VI.2. DiO labeled nanoparticles were only used for Magic Red Cathepsin L measurement, since DiD labeled nanoparticles did not produce adequate emission separation.

mCherry-GFP-LC3 retroviral expressing CMs were obtained from [3] and used in optimized settings when treated with nanoparticles for best channel separation, as determined by channel measurement of CMs with and without internalized nanoparticles. As described in Section V.6, this double-tagged fluorescent protein measurement allows autophagic flux analysis, by tracking the passage of autophagosomes that emit both GFP and mCherry fluorescence to the lysosome, upon which GFP is quenched in adequately acidified lysosomes. This assay is very well described and has great value when interpreting autophagy experiments, by allowing a direct visualization of the events that process the autophagosome, reliant on lysosomal pH [62]. This measurement is an indirect measurement of lysosomal pH, by measuring the quenching of GFP. mCherry emission was close to/but adequately separated from DiD nanoparticle stain. It was observed that higher passage number CMs displayed lower than expected amounts of green fluorescent protein (GFP) upon palmitate treatment, so experiments were optimized and performed on CMs from earlier passages 22-24. Image analysis consisted of percent of total viable CMs within one image that had GFP puncta colocalized with mCherry puncta, a measure of autophagosome flux through the lysosomal degradation pathway as described in Section V.6. For nanoparticle groups, only CMs with internalized nanoparticles were considered in this analysis, as shown in Figure A2. Two images per group per experiment were analyzed in GraphPad Prism 7 software for SEM unless otherwise noted in the figure captions.

Once collected, images were opened in LAS X (Leica) and ImageJ (National Institutes of Health) software for cellular mean intensity analysis. This was performed by drawing the outline of cells determined by comparison of increased intensity of the image in LAS X software to that of ImageJ. For example, the intensity of the image for LysoLive and LysoTracker Blue channels was increased and overlaid to best determine the cellular outline

drawn **by hand** in ImageJ. All intensities were consistent for each experiment (1 slide with 4 wells analyzed with the same image analysis settings) to ensure comparison between experimental groups. Of note, cellular outlines were only drawn of cells considered viable by observations of cell detachment and shape. For groups treated with nanoparticles, only cells with internalized nanoparticles were analyzed, as shown in Figure A1. Some multinucleated CMs were analyzed, yet most were single cells. Mean intensities were measured from the outlines and statistically analyzed in GraphPad Prism 7 software for SEM. This analysis technique was performed for **all** mean intensity data depicted in this thesis.

Cyto-ID labeling and measurement of autophagosome number was performed as per the manufacturer's protocol (Enzo 51031). Specifically, CMs were treated with for 30 minutes with the recommended concentration (no concentration data available). Epifluorescence was detected in live cells with a Leica epifluorescent microscope at 40x.

VI.5 Protein Level Measurement

Western blot analysis of protein levels within CMs was optimized from [3] on a LI-COR odyssey imager (LI-COR). Specifically, the detection of microtubule-associated protein 1 light chain 3 beta (LC3, Sigma), sequestosome-1 (p62, Cell Signaling 5114S) and glyceraldehyde-3-phasphate dehydrogenase (GAPDH, Cell Signaling 2118L) was performed by the application of primary (listed after the protein of interest) and secondary antibodies (Life Technologies A21109) on a membrane with separated denatured proteins from sodium dodecyl sulfate polyacrylamide gel electrophoresis (SDS-PAGE). CMs were lysed and scraped from 6 well plates on ice immediately after palmitate/vehicle treatment with lysis buffer containing 1x protease and phosphatase inhibitor (HALT, Fisher 78447). The protein containing supernatant from samples spun at 13.2 RPM at 4C for 20 minutes was stored at -80C until SDS-PAGE sample preparation.

Micro-BCA (Fisher 23231) was used to determine the protein concentration per sample. SDS-PAGE sample preparation consisted of the addition of 4x Laemmli sample buffer with loading dye (Bio-Rad 161-0747) to adequately diluted protein samples in lysis buffer for equal volume loading into pre-cast NuPAGE 4-12% Bis-Tris Midi Gels (Invitrogen WG1403BX10). Subsequent running and transfer onto PVDF membranes was performed for 2 and 1.5 hours respectively. Membranes were blocked with 5% w/v skim milk for 1 hour, then washed with 1x phosphate buffered saline (PBS). Primary antibody dilutions in 5% w/v BSA were added to membranes and incubated overnight at 4C. Secondary antibody labeling was performed for 1 hour, with membrane imagine performed immediately after PBS and PBS-Tween washes. Blot densitometry analysis was performed with Image Studio Lite Version 5.0 (LI-COR) and statistically analyzed in GraphPad Prizm 7 for SEM of 3 samples per experimental group for one blot.

Section VII References

1. Wende, A.R., J.D. Symons, and E.D. Abel, *Mechanisms of lipotoxicity in the cardiovascular system.* Curr Hypertens Rep, 2012. **14**(6): p. 517-31.
2. Chiu, H.C., et al., *A novel mouse model of lipotoxic cardiomyopathy.* J Clin Invest, 2001. **107**(7): p. 813-22.
3. Jaishy, B., et al., *Lipid-induced NOX2 activation inhibits autophagic flux by impairing lysosomal enzyme activity.* J Lipid Res, 2015. **56**(3): p. 546-61.
4. van Berlo, J.H. and J.D. Molkentin, *An emerging consensus on cardiac regeneration.* Nat Med, 2014. **20**(12): p. 1386-93.
5. Trudeau, K.M., et al., *Lysosome acidification by photoactivated nanoparticles restores autophagy under lipotoxicity.* J Cell Biol, 2016. **214**(1): p. 25-34.
6. Baltazar, G.C., et al., *Acidic nanoparticles are trafficked to lysosomes and restore an acidic lysosomal pH and degradative function to compromised ARPE-19 cells.* PLoS One, 2012. **7**(12): p. e49635.
7. Bourdenx, M., et al., *Nanoparticles restore lysosomal acidification defects: Implications for Parkinson and other lysosomal-related diseases.* Autophagy, 2016. **12**(3): p. 472-83.
8. Rowland, T.J., et al., *Danon disease - dysregulation of autophagy in a multisystem disorder with cardiomyopathy.* J Cell Sci, 2016. **129**(11): p. 2135-43.
9. Makadia, H.K. and S.J. Siegel, *Poly Lactic-co-Glycolic Acid (PLGA) as Biodegradable Controlled Drug Delivery Carrier.* Polymers, 2011. **3**(3): p. 1377-1397.
10. Jaishy, B. and E.D. Abel, *Lipids, Lysosomes and Autophagy.* J Lipid Res, 2016.
11. Zlobine, I., K. Gopal, and J.R. Ussher, *Lipotoxicity in obesity and diabetes-related cardiac dysfunction.* Biochim Biophys Acta, 2016. **1860**(10): p. 1555-68.
12. Riehle, C. and E.D. Abel, *Insulin Signaling and Heart Failure.* Circ Res, 2016. **118**(7): p. 1151-69.
13. World Health Organization. *Obesity and overweight fact sheet*. June 2016 [cited 2016 Sep. 8, 2016]; Available from: http://www.who.int/mediacentre/factsheets/fs311/en/.
14. Hebert, J.R., et al., *Scientific decision making, policy decisions, and the obesity pandemic.* Mayo Clin Proc, 2013. **88**(6): p. 593-604.
15. Kannel, W.B. and D.L. McGee, *Diabetes and cardiovascular disease. The Framingham study.* JAMA, 1979. **241**(19): p. 2035-8.
16. Hubert, H.B., et al., *Obesity as an Independent Risk Factor for Cardiovascular-Disease - a 26-Year Follow-up of Participants in the Framingham Heart-Study.* Circulation, 1983. **67**(5): p. 968-977.
17. Kenchaiah, S., et al., *Obesity and the risk of heart failure.* N Engl J Med, 2002. **347**(5): p. 305-13.
18. Glatz, J.F.C., et al., *CD36 as a target to prevent cardiac lipotoxicity and insulin resistance.* Prostaglandins Leukotrienes and Essential Fatty Acids, 2013. **88**(1): p. 71-77.
19. Zhang, L.Y., et al., *Cardiac diacylglycerol accumulation in high fat-fed mice is associated with impaired insulin-stimulated glucose oxidation.* Cardiovascular Research, 2011. **89**(1): p. 148-156.
20. Wende, A.R. and E.D. Abel, *Lipotoxicity in the heart.* Biochim Biophys Acta, 2010. **1801**(3): p. 311-9.
21. Opie, L.H., *Metabolism of the heart in health and disease. II.* Am Heart J, 1969. **77**(1): p. 100-22 contd.
22. Opie, L.H., *Metabolism of the heart in health and disease. I.* Am Heart J, 1968. **76**(5): p. 685-98.
23. Lopaschuk, G.D., et al., *Myocardial fatty acid metabolism in health and disease.* Physiol Rev, 2010. **90**(1): p. 207-58.
24. Neely, J.R. and H.E. Morgan, *Citation-Classic - Relationship between Carbohydrate and Lipid-Metabolism and the Energy-Balance of Heart-Muscle.* Current Contents/Life Sciences, 1987(51-52): p. 15-15.

25. Liu, L., et al., *Cardiomyocyte-specific Loss of Diacylglycerol Acyltransferase 1 (DGAT1) Reproduces the Abnormalities in Lipids Found in Severe Heart Failure.* Journal of Biological Chemistry, 2014. **289**(43): p. 29881-29891.
26. Riehle, C. and E.D. Abel, *Insulin regulation of myocardial autophagy.* Circ J, 2014. **78**(11): p. 2569-76.
27. Kaur, J. and J. Debnath, *Autophagy at the crossroads of catabolism and anabolism.* Nature Reviews Molecular Cell Biology, 2015. **16**(8): p. 461-472.
28. Jung, C.H., et al., *mTOR regulation of autophagy.* FEBS Lett, 2010. **584**(7): p. 1287-95.
29. Morita, M., et al., *mTOR coordinates protein synthesis, mitochondrial activity and proliferation.* Cell Cycle, 2015. **14**(4): p. 473-80.
30. Alers, S., et al., *Role of AMPK-mTOR-Ulk1/2 in the regulation of autophagy: cross talk, shortcuts, and feedbacks.* Mol Cell Biol, 2012. **32**(1): p. 2-11.
31. Singh, R., et al., *Autophagy regulates lipid metabolism.* Nature, 2009. **458**(7242): p. 1131-5.
32. Jiang, S., C.D. Wells, and P.J. Roach, *Starch-binding domain-containing protein 1 (Stbd1) and glycogen metabolism: Identification of the Atg8 family interacting motif (AIM) in Stbd1 required for interaction with GABARAPL1.* Biochem Biophys Res Commun, 2011. **413**(3): p. 420-5.
33. Jiang, S.X., et al., *Starch binding domain-containing protein 1/genethonin 1 is a novel participant in glycogen metabolism (vol 285, pg 34960, 2010).* Journal of Biological Chemistry, 2011. **286**(45): p. 39673-39673.
34. Reichelt, M.E., et al., *Myocardial glycophagy - A specific glycogen handling response to metabolic stress is accentuated in the female heart.* Journal of Molecular and Cellular Cardiology, 2013. **65**: p. 67-75.
35. Rabinowitz, J.D. and E. White, *Autophagy and metabolism.* Science, 2010. **330**(6009): p. 1344-8.
36. Ding, W.X. and X.M. Yin, *Mitophagy: mechanisms, pathophysiological roles, and analysis.* Biol Chem, 2012. **393**(7): p. 547-64.
37. Mancias, J.D., et al., *Quantitative proteomics identifies NCOA4 as the cargo receptor mediating ferritinophagy.* Nature, 2014. **509**(7498): p. 105-+.
38. Kroemer, G., et al., *Classification of cell death: recommendations of the Nomenclature Committee on Cell Death 2009.* Cell Death Differ, 2009. **16**(1): p. 3-11.
39. Tasdemir, E., et al., *Methods for assessing autophagy and autophagic cell death.* Methods Mol Biol, 2008. **445**: p. 29-76.
40. Park, M., et al., *Palmitate induces ER stress and autophagy in H9c2 cells: implications for apoptosis and adiponectin resistance.* J Cell Physiol, 2015. **230**(3): p. 630-9.
41. Coutinho, M.F., M.J. Prata, and S. Alves, *Mannose-6-phosphate pathway: a review on its role in lysosomal function and dysfunction.* Mol Genet Metab, 2012. **105**(4): p. 542-50.
42. Settembre, C., et al., *Signals from the lysosome: a control centre for cellular clearance and energy metabolism.* Nat Rev Mol Cell Biol, 2013. **14**(5): p. 283-96.
43. Coffey, J.W. and C. De Duve, *Digestive activity of lysosomes. I. The digestion of proteins by extracts of rat liver lysosomes.* J Biol Chem, 1968. **243**(12): p. 3255-63.
44. Ohkuma, S. and B. Poole, *Fluorescence probe measurement of the intralysosomal pH in living cells and the perturbation of pH by various agents.* Proc Natl Acad Sci U S A, 1978. **75**(7): p. 3327-31.
45. Appelqvist, H., et al., *The lysosome: from waste bag to potential therapeutic target.* J Mol Cell Biol, 2013. **5**(4): p. 214-26.
46. Beyenbach, K.W. and H. Wieczorek, *The V-type H+ ATPase: molecular structure and function, physiological roles and regulation.* J Exp Biol, 2006. **209**(Pt 4): p. 577-89.
47. Chakraborti, S. and N.S. Dhalla, *Regulation of Ca2+-ATPases, V-ATPases and F-ATPases Preface.* Regulation of Ca2+-Atpases, V-Atpases and F-Atpases, 2016. **14**: p. Ix-X.

48. Kane, P.M., *Regulation of V-ATPases by reversible disassembly.* Febs Letters, 2000. **469**(2-3): p. 137-141.
49. D'Souza R, S., et al., *Danon disease: clinical features, evaluation, and management.* Circ Heart Fail, 2014. **7**(5): p. 843-9.
50. Dehay, B., et al., *Lysosomal impairment in Parkinson's disease.* Mov Disord, 2013. **28**(6): p. 725-32.
51. Houchin, M.L. and E.M. Topp, *Chemical degradation of peptides and proteins in PLGA: a review of reactions and mechanisms.* J Pharm Sci, 2008. **97**(7): p. 2395-404.
52. Xu, Y., et al., *Polymer degradation and drug delivery in PLGA-based drug-polymer applications: A review of experiments and theories.* J Biomed Mater Res B Appl Biomater, 2016.
53. Herd, H., et al., *Nanoparticle Geometry and Surface Orientation Influence Mode of Cellular Uptake.* Acs Nano, 2013. **7**(3): p. 1961-1973.
54. Rejman, J., et al., *Size-dependent internalization of particles via the pathways of clathrin-and caveolae-mediated endocytosis.* Biochemical Journal, 2004. **377**: p. 159-169.
55. Ankrum, J.A., et al., *Engineering cells with intracellular agent-loaded microparticles to control cell phenotype.* Nat Protoc, 2014. **9**(2): p. 233-45.
56. Benjaminsen, R.V., et al., *The Possible "Proton Sponge" Effect of Polyethylenimine (PEI) Does Not Include Change in Lysosomal pH.* Molecular Therapy, 2013. **21**(1): p. 149-157.
57. Summers, H.D., et al., *Statistical analysis of nanoparticle dosing in a dynamic cellular system.* Nature Nanotechnology, 2011. **6**(3): p. 170-174.
58. Neun, B.W. and S.T. Stern, *Monitoring lysosomal activity in nanoparticle-treated cells.* Methods Mol Biol, 2011. **697**: p. 207-12.
59. GraphPad Software, I., *The SD and SEM are not the same.* GraphPad Statistics Guide, 2015.
60. Huta, B.P., et al., *The Lysosomal Protein Saposin B Binds Chloroquine.* ChemMedChem, 2016. **11**(3): p. 277-82.
61. Homewood, C.A., et al., *Lysosomes, pH and the anti-malarial action of chloroquine.* Nature, 1972. **235**(5332): p. 50-2.
62. Kliosnky, D., *Guidelines for the Use and Interpretation of Assays for Monitoring Autophagy (3rd edition) (vol 12, pg 1, 2015).* Autophagy, 2016. **12**(2): p. 443-443.
63. Mizushima, N. and T. Yoshimori, *How to interpret LC3 immunoblotting.* Autophagy, 2007. **3**(6): p. 542-545.
64. Oeste, C.L., et al., *Interactions between autophagic and endo-lysosomal markers in endothelial cells.* Histochemistry and Cell Biology, 2013. **139**(5): p. 659-670.
65. Macri, C., et al., *Modulation of deregulated chaperone-mediated autophagy by a phosphopeptide.* Autophagy, 2015. **11**(3): p. 472-86.
66. Rost, B.R., et al., *Optogenetic acidification of synaptic vesicles and lysosomes.* Nature Neuroscience, 2015. **18**(12): p. 1845-1852.
67. Dominska, M. and D.M. Dykxhoorn, *Breaking down the barriers: siRNA delivery and endosome escape.* J Cell Sci, 2010. **123**(Pt 8): p. 1183-9.
68. Lim, J., et al., *Nigericin-induced Impairment of Autophagic Flux in Neuronal Cells Is Inhibited by Overexpression of Bak.* Journal of Biological Chemistry, 2012. **287**(28): p. 23271-23282.
69. Rana, S., et al., *A spatio-temporal cardiomyocyte targeted vector system for efficient delivery of therapeutic payloads to regress cardiac hypertrophy abating bystander effect.* J Control Release, 2015. **200**: p. 167-78.
70. McCall, R.L. and R.W. Sirianni, *PLGA nanoparticles formed by single- or double-emulsion with vitamin E-TPGS.* J Vis Exp, 2013(82): p. 51015.

Appendix

This appendix contains additional figures referenced in the main body of the thesis.

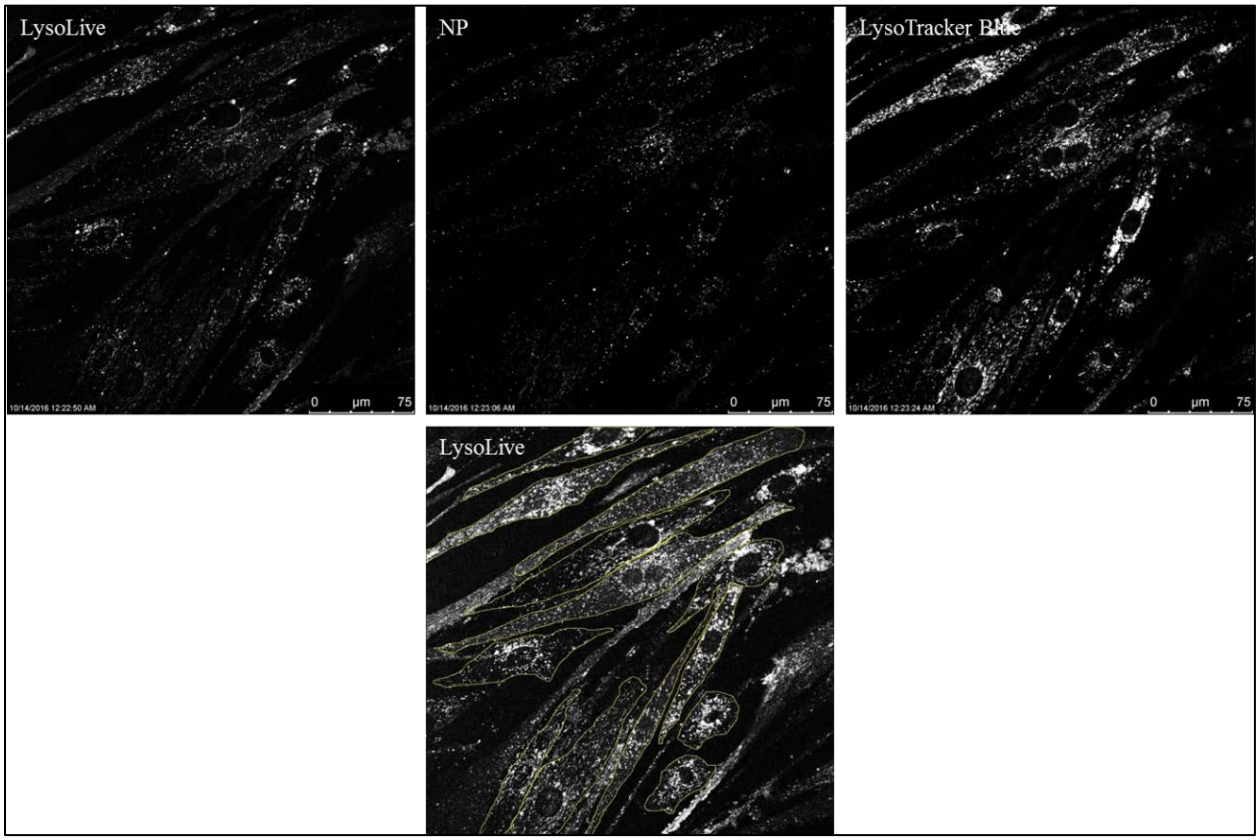

Figure A1: Image analysis of LysoLive phosphatase activity in a nanoparticle (NP) group treated with vehicle. CM outlines are shown in the lower middle image, drawn only for viable CMs with internalized nanoparticles. This image was taken after 4 hour palmitate treatment for nanoparticle (NP) **with** PEI **8 hour** pre-palmitate treatment. Note, image intensity is **increased** to best determine CM outline.

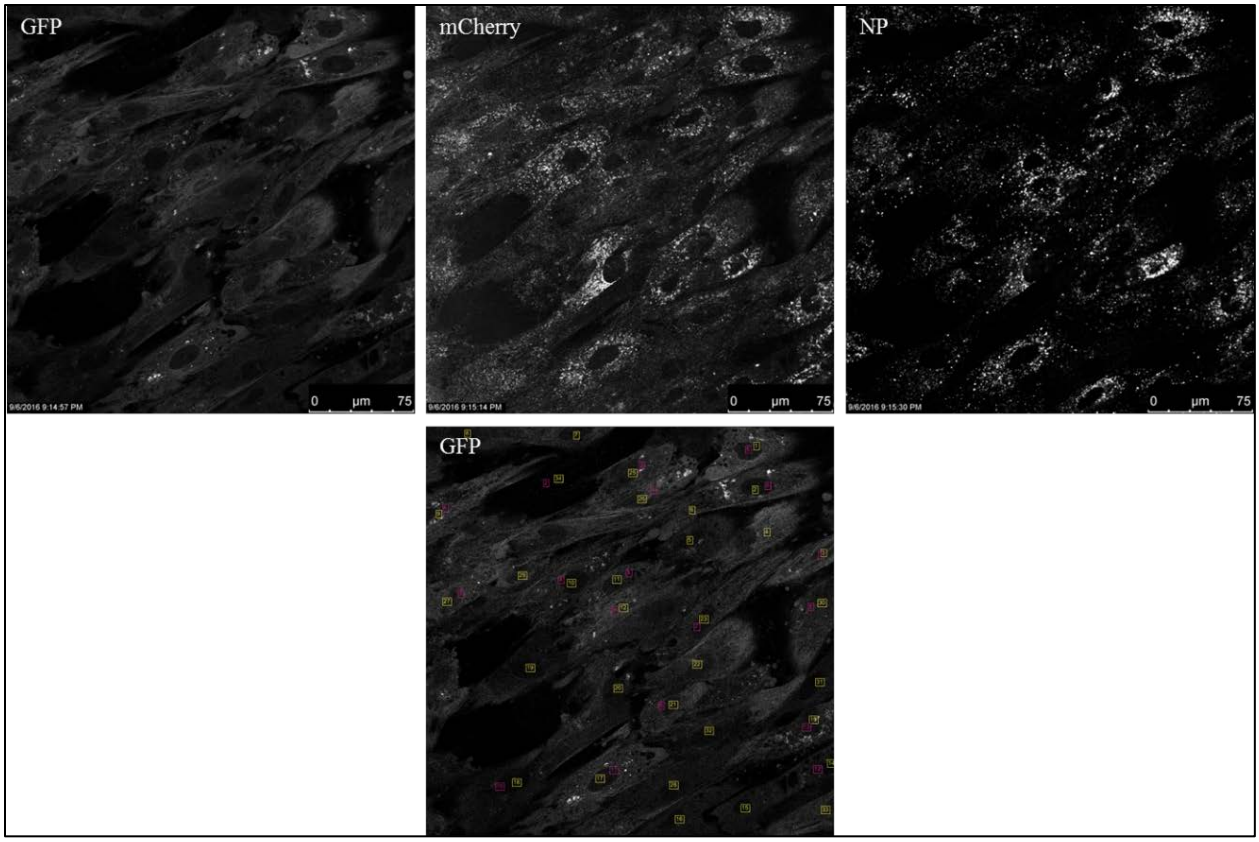

Figure A2: Image analysis of mCherry-GFP-LC3 in a nanoparticle (NP) group treated with palmitate. Cell counts are shown in the lower middle image, where yellow tags identify only viable CMs with internalized nanoparticles, and magenta tags identify CMs with GFP puncta colocalized to mCherry puncta. This image was taken after 4 hour palmitate treatment for nanoparticle (NP) **with** PEI **24 hour** pre-palmitate treatment.